Systems analysis of immune responses to attenuated *P. falciparum* malaria sporozoite vaccination reveals excessive inflammatory signatures correlating with impaired immunity

Ying Du[1]*, Nina Hertoghs[1]*, Fergal J. Duffy[1] , Jason Carnes[1], Suzanne M. McDermott[1], Maxwell L. Neal[1], Katharine V. Schwedhelm[2], M. Juliana McElrath[2], Stephen C. De Rosa[2], John D. Aitchison[1], Kenneth D. Stuart[1]

1. Center for Global Infectious Disease Research, Seattle Children's Research Institute, Seattle, WA 98019, USA
2. Vaccine and Infectious Disease Division, Fred Hutchinson Cancer Research Center, Seattle, WA 98109, USA

* Contributed equally

Abstract

Immunization with radiation-attenuated sporozoites (RAS) can confer sterilizing protection against malaria, although the mechanisms behind this protection are incompletely understood. We performed a systems biology analysis of samples from the Immunization by Mosquito with Radiation Attenuated Sporozoites IMRAS) trial, which comprised *P. falciparum* RAS-immunized (*Pf*RAS), malaria-naive participants whose protection from malaria infection was subsequently assessed by controlled human malaria infection (CHMI). Blood samples collected after initial *Pf*RAS immunization were analyzed to compare immune responses between protected and non-protected volunteers leveraging integrative analysis of whole blood RNA-seq, high parameter flow cytometry, and single cell CITEseq of PBMCs. This analysis revealed differences in early innate immune responses indicating divergent paths associated with protection. In particular, elevated levels of inflammatory responses early after the initial immunization were detrimental for the development of protective adaptive immunity. Specifically, non-classical monocytes and early type I interferon responses induced within 1 day of *Pf*RAS vaccination correlated with impaired immunity. Non-protected individuals also showed an increase in Th2 polarized T cell responses whereas we observed a trend towards increased Th1 and T-bet+ CD8 T cell responses in protected individuals. Temporal differences in genes associated with natural killer cells suggest an important role in immune regulation by these cells. These findings give insight into the immune responses that confer protection against malaria and may guide further malaria vaccine development.

Introduction

Malaria is a devastating disease that results in over 200 million cases and hundreds of thousands of deaths annually. *Plasmodium falciparum* causes the most serious disease and the most deaths, especially in sub-Saharan Africa and primarily in children (Vekemans et al., 2021). Multi-pronged efforts to eliminate malaria have led to substantial reductions in malaria incidence but the development of drug and insecticide resistance as well as other factors, including the current COVID-19 pandemic, are a challenge to further progress (Vekemans et al., 2021; Weiss et al., 2021). An effective anti-malarial vaccine has been a long term goal which has proven challenging. Currently, a single approved malaria vaccine exists, the RTS,S subunit vaccine, which elicited 28-33% protection in infants over a 4-year study period (RTSS Clinical Trials Partnership, 2015). An improved vaccine, especially one that prevents infection, would be a valuable tool in the effort to eliminate this disease. Understanding the immune responses that contribute to vaccine induced immune protection could aid the development of such vaccines.

Sporozoites (SPZs) are the liver-infectious life cycle stage of malaria, injected via mosquito bite in natural infections. Many studies in humans and model systems have shown that vaccination with *P. falciparum* SPZs that have been attenuated by radiation, genetic modification, or drug treatment can result in sterilizing immunity, as determined by subsequent controlled human malaria infection (CHMI) (Coelho et al., 2017; Obeng-Adjei et al., 2015; Portugal et al., 2015, 2014). This mode of vaccination aims to elicit immunity against pre-erythrocytic parasite stages, where the biomass of the parasites is low and the infection is asymptomatic. Currently, no universal correlates of protection have been identified and the nature of protective immunity is incompletely understood. Sterilizing immunity is likely to be complex and directed at multiple antigens given that the *P. falciparum* genome encodes more than 5,300 unique proteins. Available evidence indicates that antibodies against major surface proteins of infecting SPZs, e.g. CSP and TRAP, contribute to protection (Ishizuka et al., 2016; Seder et al., 2013). Animal models have indicated that liver-resident CD8 T cell responses are important for protection, which is inherently challenging to study in humans, as the human liver is not readily accessible for sampling and a very small fraction of its cells get infected (Fernandez-Ruiz et al., 2016b; Trieu et al., 2011). It is imperative to identify correlates of protection in humans that can aid the improvement of the current vaccines and development of vaccine candidates. To this end, human vaccination and challenge trials with attenuated *Pf*SPZs provide an opportunity to elucidate immune responses that are associated with pre-erythrocytic protection.

In this study, we applied a systems immunology approach to identify correlates of protection that are identifiable up to 28 days after initial vaccination in malaria naïve human trial subjects that participated in the Immunization by Mosquito with Radiation Attenuated Sporozoites (IMRAS)

trial (Hickey et al., 2020). Participants were immunized by *Pf*RAS delivered by mosquito bite with efficacy assessed by CHMI. Five total immunizations were delivered, spaced 4 to 5 weeks apart. The trial was designed with a suboptimal vaccine dose regime to elicit approximately 50% vaccine efficacy to facilitate comparison between protected (P) and non-protected (NP) subjects. Of particular interest in the IMRAS trial is the prime vaccination. IMRAS participants are malaria unexposed, and the initial *Pf*RAS vaccination represents the first time their immune system has been exposed to *P. falciparum* sporozoites. We hypothesized that the earliest immune resposnes to *Pf*RAS represent a critical time period determining subsequent development of sterilizing immunity.

Our integrative analysis of whole blood transcriptomics, high parameter flow cytometry and single cell CITE-seq identified numerous vaccine-induced responses including ones that correlated with protection. We observed strong negative correlations with protection that were associated with inflammation, type I interferon (IFN), and signatures related to monocytes and neutrophils, and type 2 polarized T helper cell responses. Differential kinetics in natural killer (NK) cell-associated responses and a trend of increased T-helper 1 cells correlated positively with protection. These results suggest that the priming vaccination with radiation attenuated *Pf*SPZs establishes immunological trajectories that can result in protection following additional vaccinations, and show that early inflammatory responses can negatively influence the fate of protective immunity.

Results

The IMRAS cohort analyzed consisted of eleven malaria-naïve adults immunized with five doses of approximately 200 bites from *Pf*RAS NF54 infected mosquitos (Hickey et al., 2020). The first four doses were given four weeks apart and the final dose was administered five weeks after the fourth. Protection was tested by controlled human malaria infection (CHMI) three weeks after the final vaccination (Fig. S1 A). Six of the eleven immunized participants were protected, i.e. zero parasitemia after CHMI. Of the five non-protected subjects one developed parasitemia on day 9 after CHMI and four did so on day 13 after CHMI (Fig. S1 B). There was no significant correlation between the number of *Pf*RAS infectious mosquito bites received and protection status among true-immunized subjects (Fig. S1 C).

PfSPZ vaccination induced broad transcriptome responses

Whole blood transcriptome profiling was performed on all eleven immunized IMRAS participants at 6 timepoints after the initial *Pf*RAS vaccination. We examined transcriptional changes between adjacent timepoints, which we refer to as time “intervals”, namely between days 0-1, 1-3, 3-7, 7-14, and 14-28 after immunization. We conducted linear mixed-effects regression modeling

111 analysis (LMER) of the responses to identify significantly responsive genes over all subjects and
112 those that differed between P and NP at each interval (FDR < 0.2 & p < 0.05; see Materials and
113 Methods). 90% confidence intervals (CIs) were calculated around model coefficients to label
114 genes as either increased or decreased if the CI was entirely above or below 0, respectively (Fig.
115 1A). Many significantly responsive genes were observed after the first *Pf*SPZ vaccination; 8170
116 genes had increased or decreased expression responses over at least at one interval accross all
117 immunized subjects and approximately 10% of these differed significantly between P and NP
118 subjects (Fig. 1A).
119
120 The association between vaccine induced gene responses and specific cell populations and
121 immunological processes was determined by testing whether pre-defined coherent blood
122 transcription module sets (BTMs) (Chaussabel et al., 2008a; Li et al., 2014a; Liberzon et al., 2015)
123 showed enrichment for significantly responsive genes (hypergeometric p < 0.1). We identified
124 122 BTMs significantly enriched in response genes in at least one time interval. Hierarchical
125 clustering of enriched BTM hypergeometric effect sizes at each interval revealed discrete time-
126 dependent response patterns among the immunized subjects (Fig. 1 B). BTMs increased during
127 the first day after vaccination were associated broadly with immunity and inflammation,
128 including TLR sensing; antigen processing; interferon and inflammation; monocytes and
129 neutrophils. This was accompanied by decreases in BTMs associated with the cell cycle and T
130 cells. Relatively few enriched BTMs were observed between day 1 and 3. Over subsequent
131 intervals (D3-7, D7-14, D14-28) BTMs associated with monocytes, neutrophils, TLR sensing,
132 inflammation and interferon, decreased sharply. However, we observed an increase in cell cycle-
133 associated responses from D3-7, and an induction of T cell associated BTMs at D14-28. Overall,
134 the priming vaccination resulted in robust and dynamic transcriptional responses in the
135 combined group of P and NP subjects.
136
137 ***Protection associated genes showed distinct response dynamics in P and NP individuals***
138 To further explore reponse dynamics of protection-associated genes, we performed
139 unsupervised clustering of the responses over time of the 1394 genes that were differentially
140 expressed between P and NP (FDR < 1/3 & p < 0.05, Fig.2 A; Materials and Methods). Hierarchical
141 clustering was performed separately for P and NP subjects to illustrate the response differences
142 between these two groups and to identify sets of genes with coherent response profiles over
143 time following *Pf*SPZ immunization (Fig. 2 A,C). Immune functions and molecular mechanisms
144 associated with these clusters were identified by the hypergeometric enrichment test using BTMs
145 and by Ingenuity Pathway Analysis (IPA) (see Materials and Methods) (Fig. 2 B,D, Fig. S4). We
146 identified four major gene clusters for P subjects (P_1, P_2, P_3, P_4) and five for NP subjects
147 (NP_1, NP_2, NP_3, NP_4, NP_5). The patterns in which these 1394 genes changed over time
148 differed between P and NP, leading to substantial differences in gene composition of most of the

149 major P and NP clusters (Fig.2 A,C,E). A total of 39 signficantly enriched BTMs and 159 significant
150 IPA pathways were identified between P and NP (Table S1).
151
152 Most gene clusters from both P and NP were strongly enriched for cell cycle-associated BTMs
153 (Fig.2 B,D). An important exception was P_1 and NP_1, both were associated primarily with
154 various immune response modules including many type I IFN-associated modules. These two
155 gene clusters have the largest total numbers of genes and associated BTMs. In total, P_1 and
156 NP_1 have 317 genes in common (hypergeometric p = 4.2e-17) (Fig. 2 E), although numbers of
157 enriched modules and gene expression dynamics are distinct (Fig. S2 A-C). Expression of most
158 genes in these clusters was increased over the interval D0-1, with higher response magnitude in
159 NP_1 (Fig. S2 C). Consistent with strong enrichment of type I IFN associated modules in P and NP-
160 associated cluster 1, we observed that IFN-stimulated genes (ISGs) were strongly increased
161 overall in NP compared with P and NP by day 1 after the first vaccination (Fig.2 F, Mann Whitney
162 U test, P < NP, p < 2.2e-16) (Kazmin et al., 2017). Furthermore, we observed significantly
163 increased expression of genes related to sensing through Pattern Recognition Receptors (PRR) in
164 NP participants by day 1, for both MyD88 dependent and independent pathways (Fig. S3 A-C).
165 Altogether, these patterns indicate that overall innate sensing and inflammatory responses were
166 highly elevated in NP compared to P subjects, strongly suggesting that they negatively affected
167 the induction of adaptive immunity against SPZ challenge.

168 ***Gene set enrichment analysis identified early inflammation as correlate of impaired immunity***
169 To more broadly explore immunological processes and cell types associated with protection we
170 performed gene set enrichment analysis (GSEA) separately for P and NP subjects at each time
171 interval (Fig. 3 A). GSEA facilitated identifying important coherent response modules that our
172 above analysis based on differentially expressed genes may not have revealed. GSEA revealed 80
173 BTMs significantly enriched at one or more timepoints (FDR < 0.1). Twenty of these BTMs
174 overlapped with the 39 BTMs enriched in differentially expressed genes.

175 Patterns of responses over time differed between P and NP. Two modules showed opposite
176 responses: *M4.0 cell cycle transcription* over day 0-1, and *M196 platelet activation + actin binding*
177 over day 3-7 were both increased in P and decreased in NP. Hierarchical clustering of the GSEA
178 BTM normalized enrichment scores (NESs) identified four major clusters of BTMs (Fig. 3 A) and
179 many of the BTMs within a cluster shared genes (Fig. 3 B). GSEA cluster 1 is associated with B and
180 T cells, cluster 2 with cell cycle and potentially cell proliferation, cluster 3 with NK cells, and
181 cluster 4 with monocytes, neutrophils and immune activation.

182 Cluster 1 contained BTMs associated with T and B cells. These BTMs decreased over day 0-1
183 specifically in NP, with most BTMs remaining unchanged at all other time intervals for both P and
184 NP. BTMs in cluster 2 were generally associated with cell cycle and division. These BTMs were
185 downregulated over day 0-1 and day 7-14 and upregulated from day 3-7 in both P and NP.

186 Notably, most of these BTMs were activated in NP but not in P from day 3-7. Cluster 3 was the
187 most heterogeneous cluster in terms of composition and time dynamics, and included NK cell,
188 plasma cell and trancriptional regulatory BTMs among others. These modules tended to be
189 increased at early time intervals, before decreasing at day 7-14 and day 14-28. Notably, NK BTMs
190 were upregulated in P over day 0-1; however, their activation occurred late in NP over day 1-3
191 and day 3-7. Cluster 4 primarily represented innate inflammation, interferon, monocytes,
192 neutrophils and dendritic cell BTMs. Consistent with our above gene-based analysis, cluster 4
193 responses in NP individuals increased sharply at day 0-1 and day 7-14 with an intermediate
194 decrease from day 3-7, with relatively few changes in P individuals over the first four time
195 intervals. Both P and NP individuals showed decreased responses in cluster 4 BTMs day 14-28.
196 Cluster 4 also included platelet BTMs, and early activation of platelets in NP may reflect their
197 influence on the elevated expression associated with immune activation and monocytes (Rolfes
198 et al., 2019). Activated neutrophils produce reactive oxygen species (ROS), and we observed an
199 increase in ROS signalling in NP (Fig. S5 A-C) at day 0-1. The differences between P and NP subjects
200 in this cluster highlights the greater magnitude of inflammatory responses by innate cells in NP
201 versus P subjects early after the first immunization. Overall, this analysis supports our hypothesis
202 that high levels of inflammatory responses and type I IFN are detrimental for protective
203 immunity, and suggests these responses are associated with monocytes, DCs and NK cells.
204
205 ***Specific Immune cell types associated with protection by trancriptomics and flow cytometry***
206 GSEA and differential gene expression analyses indicated that specific immune associated
207 transcriptional responses were induced at different times and to different extents between P and
208 NP subjects. This suggests that specific immune cell populations responded differently in P vs NP,
209 thus, we further investigated whether a cell type-specific signature could be identified after initial
210 *Pf*RAS immunization.
211
212 We generated heatmaps of expression changes by averaging expression of genes from significant
213 cell-type associated BTMs identified by the GSEA analysis (Fig. 4 A,B, Fig. S6 A-G). Monocytes,
214 DCs, neutrophils and platelet-associated responses were highly increased in NP over day 0-1,
215 indicating strong innate immune responses in NP that were absent or significantly lower in P
216 subjects (Fig. 4 A,B, Fig. S6 A-D). In contrast, genes associated with T and B cells were strongly
217 decreased over day 0-1 in NP subjects (Fig. 4 A, Fig. S6 E-F). Both P and NP subjects had a modest
218 increase in B cell associated genes in the last time interval (Fig. S6 F). Interestingly, P and NP
219 subjects differed in the timing, magnitude and nature of active NK cell-related genes (Fig. 4 A).
220 Once again, these results indicate that early innate immune activation strongly correlates with
221 insufficient immunity to challenge after the completion of the vaccine regimen and
222 transcriptome responses associated with adaptive cell types show the opposite expression
223 pattern.

224
225 To validate this whole blood transcriptional analysis, we applied high parameter flow cytometry
226 to characterize PBMCs isolated from immunized individuals after the first immunization. This was
227 done at overlapping time points with the whole blood transcriptional analyses, although we
228 lacked matching PBMC samples for the 1 day and 28 days post immunization timepoints (Table
229 S2, Fig.5 A-G). We assessed whether transcriptional responses associated with specific cell types
230 were correlated with flow cytometry derived counts of the appropriate populations.
231
232 Consistent with the RNAseq data, NP subjects showed a trend towards increased numbers of
233 circulating monocytes shortly after the first immunization, specifically non-classical monocytes
234 (CD14+-CD16+) (Fig5A, p = 0.06). These inflammatory cells have been implicated in several
235 vaccination studies to be correlated with impaired immunity (George et al., 2018; Mitchell et al.,
236 2012). We also observed increased numbers of ILT3+ monocytes, associated with IFN exposure
237 (Jensen et al., 2010; Waschbisch et al., 2014), after the first vaccination (Fig.5 A, p = 0.0004).
238 Furthermore, by applying a previously identified transcriptional signature of macrophage
239 polarization (Becker et al., 2015), we observed that responses associated with classically
240 activated macrophages were specifically increased in NP between day 0-1, but no change was
241 observed for alternatively activated macrophage responses (Fig S6 H,I). We compared the
242 abundance and activation status of several DC subsets between P and NP subjects and found
243 several trends that were consistent with RNA-seq results, albeit not statistically significant (Fig. 5
244 E). We observed a subtle increase in plasmacytoid DCs, and overall increased CD11c+ DC numbers
245 3 days after the first immunization in NP compared to P subjects (Fig. 5 B). Interestingly, the
246 proportion of "mature" CD1c+ DCs expressing CD86 was higher in P than NP subjects whereas
247 CD86 expressing CD11c+ DCs that lack CD1c or CD141 expression, and non-activated CD1c DCs
248 were enriched in NP subjects. These findings suggest that CD11c+ DCs, non-activated CD1c+ DCs
249 and non-classical monocytes contribute to the transcriptional signature in NP subjects where we
250 observed an increase in DC and monocyte-associated genes (Fig.5 B, Fig. 4 A, Fig. S6 B,H,I).
251 Because different types of DCs can activate and skew different T-helper cell responses, we also
252 assessed the proportion of Th1 and Th2 CD4+ T cells (Collin and Bigley, 2018) and observed
253 greater proportions of Th2 CD4 T cells in NP, and a trend towards more Th1 cells in P subjects
254 (Fig. 5C). In addition, we found a trend of higher circulating numbers of CD8 T cells and T-bet
255 expressing CD8 T cells in P subjects. In CD8 T cells, T-bet is an important transcription factor that
256 is involved in memory cell formation (Sullivan et al., 2003). These data suggest that differences
257 in innate responses contributed to impaired protective immunity by skewing the CD4 T cells
258 toward a type 2 phenotype, and protective responses are hallmarked by Th1 and CD8 T cell
259 responses. The abundance of the NK cells in general, and CD38 expressing NK cells matched the
260 transcriptome responses in which NK-associated gene increases peaked at day 1-3 in P subjects
261 and day 7 in NP subjects (Fig. 5D). However CD8-expressing NK cells subsets did not show any

262 early peak in P participants. Notably, CD8+ NK cells lacking FcRγ were more abundant in NP
263 subjects across all measured timepoints (Hart et al., 2019; Hwang et al., 2012; McKinney et al.,
264 2021; Zambello et al., 2020).
265
266 To quantify the relationships between the transcriptional and cytometric data, we performed
267 correlation analysis of temporal changes of BTMs and cell subsets from manually gated flow
268 cytometry data (Fig. 6 A). These analyses showed that transcriptional activation of the innate
269 immune response (inflammatory responses, monocyte signatures, DC signatures, viral sensing &
270 immunity, antigen processing & presentation, etc.) positively correlated with increases in the
271 proportion of innate immune cells (DCs, monocytes) (Fig. 6 B). In contrast, transcriptional down-
272 regulation of T cell-related responses (T cell activation, T cell differentiation) paralleled cellular
273 decreases of CD3 T cells (Fig.6B), and transcriptional activation of several NK-associated genes
274 positively correlated with increases in NK cells (Fig. 6 B). The activation of innate immune
275 responses (increases in BTMs related to monocytes, DCs, inflammatory responses) in NP subjects
276 correlated with decreases in total T cell counts (Fig. 6 C). The down-regulation of T cell modules
277 (T cell activation, T cell differentiation) was associated with increases in the abundance of DCs
278 and monocytes (Fig. 6 C). Additionally, the downregulation of B cell-associated genes was
279 correlated with cell composition increases in NKT-like cells that co-express CD3 and CD56 (Fig. 6
280 C). These analyses indicate that the transcriptional data and the flow cytometry data align
281 consistently and reveal cell abundance and activation changes that correlate with each other.
282
283 ***RNAseq and flow cytometry findings were further validated with scRNAseq***
284 To further validate the identity of cell subsets indicated by transcriptional analysis, we performed
285 CITEseq with a panel of 14 antibodies using PBMC samples collected on day 0, day 3 and day 14
286 after the priming dose of *Pf*SPZ from an IMRAS subject who dropped out of the trial (Table S3).
287 We obtained single cell RNA seq gene expression and surface protein marker profile data from a
288 total of 12,442 cells. Mapping of these cells to a previously defined multimodal cell atlas based
289 on reference clusters identified 29 cell types in the merged samples (Fig. 7 A) (Hao et al., 2021).
290 We then derived transcriptional cell-type associated signatures using genes highly expressed in
291 CITEseq-identified cell types in our samples, and applied these signatures in GSEA analysis of the
292 whole blood RNA-seq data (Fig. 7 B). Consistent with previous BTM-based GSEA analyses, GSEA
293 with our CITEseq signatures indicated that CD14+ and CD16+ monocyte subsets were highly
294 activated on day 1 in NP subjects. By contrast, genes associated with NK cells were highly
295 activated on day 1 in P subjects, whereas the activation continued on day 3 in NP subjects (Fig. 7
296 B,C). Finally, comprehensive correlation analysis was performed to examine the relationship
297 between cell subsets predicted by CITEseq and cell-specific BTMs identified in our previous GSEA
298 (Fig. 3, Fig. 4). The high correlation between cell-specific BTMs and corresponding cell types
299 identified in CITEseq data demonstrates that the cell subsets identified by both approaches are

300 consistent (Fig. 7 D) and supports our interpretation of these responses. Thus, integration of
301 whole blood RNA-seq, high parameter flow cytometry and scRNA-seq of individuals after initial
302 *Pf*RAS vaccination revealed a consistent picture where inflammatory transcripts and non-classical
303 monocytes, and Th2 signalling are specifically increased in NP individuals in the first day after
304 *Pf*RAS vaccination while P individuals are marked by increased early NK-cell and Th1 signalling.
305

306 **Discussion**

307 Whole blood transcriptome, high parameter flow cytometry and CITEseq systems analyses of the
308 IMRAS trial identified numerous responses to the first vaccination, including early inflammatory
309 responses that correlated with a lack of protection. These early inflammatory responses were
310 associated with myeloid cells, including neutrophils and increased levels of monocyte and DC
311 subsets, and Th2 cells. This substantial early inflammatory stimulation may have resulted in
312 skewing toward a type 2 response. In contrast, effective protection was correlated with early
313 responses associated with NK cells, later responses associated with T cells and lower overall
314 responses. These results underscore the influence of early innate and adaptive responses on the
315 subsequent immunological trajectories as shown by different response profiles that do or do not
316 ultimately lead to protection from infection (Figs. 2,3). We hypothesize that differential priming
317 of the adaptive compartment by PfRAS vaccinations impacts subsequent responses and
318 ultimately protection from infection by protected vs not protected vaccinees. Thus, immune
319 responses to the first vaccination may be decisive for the outcomes of vaccinations with
320 attenuated sporozoites and may provide early biomarkers of protection.

321 Myeloid cell activation as a negative correlate of protection may seem counterintuitive since
322 activation is required for antigen presenting cell (APC) priming of adaptive T cell responses in
323 lymphoid tissues. The higher levels of inflammatory responses that we found to correlate with a
324 lack of protection in this study imply that over-induction of inflammation negatively impacted
325 the development of protective adaptive responses. Previously, innate pathways that suppress
326 adaptive responses have been identified in the context of immune pathology (Minkah et al.,
327 2019; Wherry et al., 2007). Similarly, the early increase in neutrophil-associated gene expression
328 following vaccination correlated with a lack of protection. Although neutrophils are rapid innate
329 responders to infection and function in pathogen clearance and immune modulation (Mantovani
330 et al., 2011), a subset of neutrophils that are systemically induced upon acute inflammation
331 suppress T cell responses through ROS production (Kusmartsev et al., 2004; Pillay et al., 2012;
332 Zemans, 2018). The increased expression of transcripts associated with ROS production observed
333 in NP subjects implies that neutrophil suppression of T cell responses may also have negatively
334 impacted development of protective adaptive immune responses after PfRAS vaccination.
335

336 Innate priming of naïve T cells into various T-helper cells can occur through the actions of
337 neutrophils and basophils, DC subsets via their intrinsic properties or their interplay with other
338 innate cells, including the induction of Th2 cells in response to type 2 innate lymphoid cell (ILC2)-
339 derived cytokines (Kim and Kim, 2018; Otsuka et al., 2013; Phythian-Adams et al., 2010; Tang et
340 al., 2010; Tjota and Sperling, 2014). The reciprocal early relative increase in Th2 cells and
341 decrease in Th1 cells in NP subjects only implies that inhibition of polarization of Th1 cells by Th2
342 cytokines suppressed development of responses that protect against CHMI (Kim and Kim, 2018).

343 We also observed a trend towards higher numbers of Th1 and CD8 T cells in P vs NP subjects at
344 early timepoints, suggesting that Th1 responses contribute to PfRAS vaccination-induced
345 immunity. This is consistent with studies in animal models which concluded that sterilizing
346 protection involves Th1 cells which secrete IFNγ and, in co-ordination with with macrophages
347 and liver resident cytotoxic CD8 T cells, eliminate intracellular pathogens (Cockburn et al., 2013;
348 Fernandez-Ruiz et al., 2016a; Hickey et al., 2020; McNamara et al., 2017; Tse et al., 2014)(Perez-
349 Mazliah and Langhorne, 2014). In addition, the correlation of CSP-specific, IFNγ-producing CD4 T
350 cells with protection from infection following RTS,S/AS02 vaccination (Reece et al., 2004) also
351 suggests that Th1 cells can contribute protective immunity in humans.
352
353 Increases in monocyte associated transcriptome responses and of non-classical and ILT3-
354 expressing monocytes in NP subjects suggest that these responses impair development of
355 protection following Pf vaccination. Impairment of vaccine elicited immunity has been linked to
356 non-classical or inflammatory monocytes in mice (George et al., 2018; Li et al., 2013; Mitchell et
357 al., 2012) perhaps involving ILT3 monocyte recruitment to lymph nodes and interference with T
358 cell priming as implied by the enhanced T cell priming following monocyte depletion. GM-CSF
359 production by monocytes and sequestration of cysteine have been suggested as mechanisms of
360 T cell suppression during priming (Mitchell et al., 2012; Serafini et al., 2004). The correlation
361 between type I IFN expression and the lack of protection that observed in this work (Fig 2F) and
362 in a vaccine trial of malaria SPZs given under chemoprophylaxis cover (Tran et al., 2019) indicates
363 that these responses can hamper the development of adaptive responses. That ILT3 surface
364 expression by monocytes can result from type I IFN stimulation (Jensen et al., 2010; Waschbisch
365 et al., 2014) and both type I IFN and ISGs increased expression in NP subjects early after
366 vaccination suggests that the monocytes in NP subjects have encountered type I IFN stimulation.
367 Type I IFNs are potent immune mediators that can directly activate DCs, NK cells and T and B cells
368 and regulate immune responses to many pathogens. These IFNs signal through the interferon
369 alpha receptor (IFNAR) that is present on almost all cells in the body and induce ISGs that function
370 in the control of infection. However, type I IFN has also been linked to immune pathology in
371 chronic viral diseases and in some bacterial infections (McNab et al., 2015). The ultimate
372 protective vs non protective effects of the type I IFN response may well depend on its timing,
373 localization and magnitude of the specific IFN responses as has been suggested (Nagai et al.,
374 2003).
375
376 Protection elicited by vaccination with radiation attenuated SPZs requires an abortive liver
377 infection (Doolan and Hoffman, 2000). Infection studies in animals have shown that malaria
378 infected hepatocytes produce type I IFN, and IFNγ-secreting NK and NKT cells are recruited as
379 liver stage parasites are eliminated (Miller et al., 2014). However, type I IFN responses are also
380 detrimental to long term immunity against infection (Liehl et al., 2015, 2014; Miller et al., 2014;

381 Minkah et al., 2019). Caspase-mediated cell death of infected hepatocytes is required for the
382 uptake and presentation of malaria antigens by innate phagocytic cells (Kaushansky et al., 2013;
383 Kurup et al., 2019; Marques-Da-Silva et al., 2021) but type I IFN can inhibit caspase activity and
384 inflammasome activation thus potentially inhibiting the presentation of malaria antigens (Guarda
385 et al., 2011; Veeranki et al., 2011). IFNAR signaling during malaria liver infection may also impair
386 the induction of Th1 and CD8 T cell responses and enhance exhaustion of liver resident CD8 T
387 cells (Haque et al., 2014; Minkah et al., 2019; Nagai et al., 2003). In addition, type I IFN can
388 hamper protective immunity via inhibition of IFNγ responsiveness by monocytes and
389 macrophages that in turn can limit the induction of Th1 responses (de Paus et al., 2013;
390 Rayamajhi et al., 2010). Overall IFNγ is an important mediator in anti-malarial immunity with a
391 variety of downstream effects besides macrophage activation (King and Lamb, 2015). We did not
392 find that the best known and potent producers of large quantities of type I IFN, namely
393 plasmacytoid DCs (pDCs), had significantly higher levels of in NP subjects; however, other innate
394 cells, e.g. neutrophils, monocytes and DCs can secrete type I IFN (Ali et al., 2019; Rocha et al.,
395 2015).
396
397 NK cell-associated transcriptome responses (Figs 3A and 4A) and relative changes in NK cell
398 subset numbers (Fig 6B) occur earlier in P than in NP subjects, which may indicate that they
399 contribute to the development of immunity, perhaps via the balance between Th1 and Th2
400 responses. NK cells can be activated by neutrophils as well as inflammatory monocytes through
401 type I IFN (Costantini and Cassatella, 2011; Lee et al., 2017) and they can have diverse functions.
402 They can act as immune regulators that enhance or suppress adaptive responses and they can
403 be innate effectors that rapidly respond to and eliminate infected or tumor cells (Schuster et al.,
404 2016; Vivier et al., 2008). IFNγ secretion by NK cells can support DC-mediated Th1 induction
405 (Schuster et al., 2016; Zhao et al., 2020), analogous to that we observed in P subjects, but NK cells
406 can also limit adaptive responses by suppressing DCs, CD4 T cells and B cells and thus variably
407 impact outcomes (Hayakawa et al., 2004; Piccioli et al., 2002; Zhang et al., 2013; Zhao et al.,
408 2020). Furthermore, NK cells can reduce inflammation, e.g. as with COVID-19 related immune
409 pathology (Li et al., 2020; Mehta et al., 2020; van Eeden et al., 2020; Zheng et al., 2020). Thus,
410 the early NK responses in P subjects may support the priming of a Th1 polarized response and
411 inhibit inflammation that in NP subjects primes a Th2 response. Interestingly, we identified a
412 novel NK cell subset that expressed CD8 and lacked FcRγ expression and which is more abundant
413 in NP subjects in the day 3-7 interval (Fig. 5D). FcRγ-lacking NKs have previously been associated
414 with an adaptive phenotype that is protective against seasonal malaria infection (Hart et al.,
415 2019). Further investigations into this phenotype could elucidate its functionality.
416
417 Overall, our analyses indicate that early innate responses to live irradiation attenuated SPZ
418 vaccination substantially impact the development of adaptive responses and ultimately

419 protection from malaria infection. Understanding mechanisms of protection is complicated by
420 the likelihood that protective effector processes are multi-functional, due to the large breadth of
421 potential antigens, and protection may occur at multiple points between the introduction of SPZs
422 and the establishment of a blood stage infection. Both antibody and cellular mediated
423 mechanisms may contribute to protection: monoclonal antibodies derived from attenuated SPZ
424 vaccination can protect humanized mice although antibody levels variably correlate with
425 protection (Epstein et al., 2017; Hickey et al., 2020) and liver resident CD8+ T-cells and IFNγ
426 correlate with protection in non-human primates (Pichyangkul et al., 2017). The complex balance
427 of responses associated with protection are illustrated here by the differential early inflammatory
428 responses between P and NP subjects and the potential effects on Th1 and Th2 responses. The
429 events following the priming vaccination that correlated with protection are early NK associated
430 responses in the context of limited inflammatory responses followed by CD4+ T cell responses
431 and subsequently CD8+ T cell responses.
432
433 That this study was performed on blood samples, despite decisive immune events occuring in the
434 liver, which is essentially experimentally inaccessible, limited us to indirect analysis of phenotypic
435 differences between the P and NP subjects rather than functional assays. The sample size is
436 relatively small, which reduced our sensitivity to discover more subtle changes associated with
437 protection, especially given natural variation in the participants. However, the detection of
438 robust correlates of protection despite the low numbers increases our confidence that we have
439 identified meaningful responses. These findings can inform further studies to extend the
440 understanding of protective immunity and its development. In addition, multiple factors may
441 have influenced the differences that between P and NP subjects that we described here, and
442 which influenced protection. These include intrinsic differences between subjects, such as HLA
443 type and other genetic differences as well as baseline immune status at the time of immunization.
444 Also vaccination via infected mosquito bites may have contributed to variability in the effective
445 vaccine dose received by each participant, i.e. the number of liver cells infected by live
446 attenuated SPZs. In addition, the point at which parasite development in the liver cells was
447 arrested may have been variable since radiation damage is random which may have impacted
448 the amount and type of parasite antigen available for presentation.
449
450 In conclusion, we show that a strong acute inflammatory response to a priming vaccination
451 correlates with the ultimate lack of protection in this trial of malaria naive volunteers. We
452 hypothesize that this results in skewing adaptive responses toward Th2-centered responses
453 rather than protective Th1 responses and that this similarly impacts responses to subsequent
454 immunizations. Thus, immune responses to the first vaccination can be decisive for the outcome
455 of the trial.
456

Materials and Methods

Sample collection and RNA sequencing

Whole blood was collected from IMRAS trial participants directly into PAXgene blood RNA tubes (PreAnalytiX, Hombrechtikon, Switzerland) and stored at −20 °C. RNA extraction and globin transcript depletion (GlobinClear, ThermoFisher Scientific, MA, USA) were performed prior to cDNA library preparation using the Illumina TruSeq Stranded mRNA sample preparation kit (Illumina, CA, USA). Globin transcript depletion, cDNA library preparation and RNA sequencing were performed by Beijing Genomics Institute (Shenzhen, China). A total of sixty-six RNA-seq samples were sequenced, with a target depth of 30 million reads per sample. Eleven of the samples were sequenced on Illumina (San Diego, CA) Hiseq2000 sequencers using 75 base-pair (bp) paired-end reads. The remaining one hundred and eighty-six samples were sequenced on BGI500 sequencers using 100 bp paired-end reads.

Quality control and processing of RNA-Seq data

RNA-seq data were processed as previously described (Thompson et al., 2017). Read pairs were adjusted to set base calls with phred scores < 5 to 'N'. Read pairs for which either end had fewer than 30 unambiguous base calls were removed, a method that indirectly removes pairs containing mostly adaptor sequences. Read pairs were aligned to the human genome (hg19) using STAR (v2.3.1d) (Dobin et al., 2013). Gene count tables were generated using htseq (v. 0.6.0) with the intersection-strict setting on and Ensembl gene annotations (GRCh37.74) used to link genomic locations to gene identifiers (Anders et al., 2015). Log2-transformed TMM-normalized counts-per-million (CPM) expression matrices were computed using the cpm function of the edgeR package (McCarthy et al., 2012). Batch correction for sequencer model (Hiseq2000vs BGI5000) was performed on log2-transformed counts using linear mixed-effects models with normally distributed errors and an unstructured covariance matrix. Mixed-effects models were fit using the R (https://www.r-project.org/) Lme4 package (Bates et al., 2015). The following formula was used:

$$\text{EXPRESSION} = \text{SEQUENCER} + (1|\text{PARTICIPANT})$$

in which EXPRESSION represents the log2-transformed CPM value, SEQUENCER the sequencing platform, and including random intercepts for each PARTICIPANT. To create a final batch-corrected expression matrix, raw CPMs were adjusted by subtracting the fitted SEQUENCER coefficient.

492 **Mixed-effects modeling to identify transcriptional signatures that were regulated by the**
493 **primary vaccine and responded differentially in protected and non-protected immunized**
494 **participants**
495 Linear mixed-effects regression models (LMER) were used to model individual gene expression
496 (EXPRESSION) as a function of sample collection time (TIME) and protection after CHMI
497 (PROTECTION), with TIME and EXPRESSION as fixed effects, and PARTICIPANT as a random effect.
498
499 Mixed-models were fit as follows:
500 Full model: EXPRESSION ~ TIME + PROTECTION + TIME:PROTECTION + (1|PARTICIPANT)
501 Reduced model 1: EXPRESSION ~ PROTECTION + (1| PARTICIPANT)
502 Reduced model 2: EXPRESSION ~ TIME + (1| PARTICIPANT)
503
504 By contrasting the full model with reduced models lacking the TIME and PROTECTION terms, the
505 significance of relationships between the TIME and PROTECTION variables and EXPRESSION were
506 evaluated. ANOVA was used to compare the full model with reduced model 1, where *P*-values
507 represent the significance of the improvement of fit associated with the TIME term in the
508 analysis. FDR-adjusted *P*-values were computed using the Benjamini-Hochberg method.
509 PROTECTION-associated genes were similarly identified within the TIME significant genes using
510 ANOVA to compare the full model with reduced model 2.
511
512 To identify genes with significant changes in EXPRESSION at specific time points relative to the
513 pre-vaccination state, five full models were fit for each gene with two time points (each time
514 point following vaccination 1 and its previous time point, i.e. time intervals) included in the TIME
515 term. In addition, for each gene, models were fit that included all time points (Days 0,1,3,7,14,28)
516 to identify transcriptional signatures that had temporal effects at any time point.
517
518 To determine the direction (UP/DOWN) of transcriptional responses relative to either pre-
519 vaccination time point or the previous time point in all immunized subjects, 90% confidence
520 intervals were estimated for the TIME coefficient of the reduced model 2 as above. Cases where
521 the lower CI > 0 were considered UP genes, upper CI < 0 were considered DOWN genes.
522
523 **Mixed-effects modeling to identify cell types that had significantly different cell proportion**
524 **changes in P and NP immunized participants after the primary vaccination**
525 Linear mixed-effects regression models (LMER) were used to model individual cell type
526 proportion (PERCENTAGE) as a function of sample collection time (TIME) and protection after
527 CHMI (PROTECTION), with TIME and PERCENTAGE as fixed effects, and PARTICIPANT as a random
528 effect.
529

530 Mixed-models were fit as follows:
531 Full model: PERCENTAGE ~ TIME + PROTECTION + TIME:PROTECTION + (1|PARTICIPANT)
532 Reduced model 1: PERCENTAGE ~ TIME + (1| PARTICIPANT)
533
534 By contrasting the full model with reduced models lacking the PROTECTION terms, the
535 significance of relationships between the PROTECTION variables and PERCENTAGE were
536 evaluated. ANOVA was used to compare the full model with reduced model 1, where *P*-values
537 represent the significance of the improvement of fit associated with the PROTECTION term in the
538 analysis.
539
540 **Gene set enrichment analysis (GSEA)**
541 GSEA was performed for each vaccination time interval using the R fgsea package (Korotkevich
542 et al., 2016; Mootha et al., 2003; Subramanian et al., 2005) with 500 permutations and whole
543 blood transcriptional modules (Chaussabel et al., 2008b; Li et al., 2014b; Subramanian et al.,
544 2005; Tran et al., 2019). Genes were ranked by average fold change across each time interval
545 (day 1 to day 0, day 3 to day 1, day 7 to day 3, day 14 to day 7, day 28 to day 14) separately for
546 samples from P and NP subjects. Normalized enrichment scores (NES) of non-significant modules
547 (FDR-adjusted *P*-value > 0.05) were set to 0.
548
549 **Statistical tests**
550 The hypergeometric test was used to identify BTM modules enriched for subsets of genes. The
551 resultant effect size (ES) was calculated as: (b/n)/(B/N), in which n: Number of genes of interest;
552 N: Number of total mapped genes; b: Number of genes of interest from the given module; B:
553 Number of genes from the module in the total mapped genes.
554
555 Ingenuity pathway analysis (IPA) was performed using the IPA software from Qiagen. *P*-values
556 were calculated using Fisher's Exact Test and FDR-adjusted P-values < 0.1 were considered
557 significant.
558
559 **Unsupervised clustering**
560 Hierarchical clustering of summary measures representing gene expression/responses (average
561 gene fold changes, GSEA NES, or ES scores) was computed by agglomerative complete linkage
562 with 1 - (Pearson's correlation coefficient) as the distance metric. The optimal number of clusters
563 was determined by the "elbow" method (Thorndike, 1953).
564
565 **Flow cytometry data**
566 PBMCs were collected from IMRAS participants on day 0, and 3, 7 and 14 after the first
567 immunization and frozen for later use. After thawing in RPMI supplemented with 10% FBS and

568 benzonase nuclease (Millipore EMD 0.05 U/ml), the samples were incubated with LIVE/DEAD™
569 Fixable Blue Dead Cell Stain Kit and the Human BD Fc Block for 30 min at room temperature
570 before being simultaneously stained with four phenotyping panels that have been previously
571 described in OMIP-044 and OMIP-064 and further described in Table S2 (Hertoghs et al., 2020;
572 Mair and Prlic, 2018). The cells were then acquired using a BD FACSymphony flow cytometer. The
573 data were analyzed, and cellular populations gated and quantified using FlowJo Software (version
574 9.6.6). The percentage contribution of each manually gated cell subset was calculated using the
575 counts of each defined cell subset divided by the total single live cells from that sample. Pearson
576 correlation coefficients were calculated between cell type proportion changes and BTM mean
577 expression level changes per-time interval for P an NP subjects separately.

578

579 **CITE-seq single-cell RNA seq processing**

580 Live frozen PBMCs were obtained from a single vaccinated individual in cohort 1 of the IMRAS
581 trial at day 0, and three- and 14-days post first vaccination. Cells were thawed and washed with
582 RPMI supplemented with 10% FBS and benzonase nuclease (Millipore EMD 0.05 U/ml). PBMCs
583 were resuspended in 100 µl of PBS supplemented with 2% w/v Fetal Bovine Serum (FBS) and
584 incubated with Fixable Viability Stain 510 and Human BD Fc Block for 30 minutes at room
585 temperature. Cells were washed with 2% FBS PBS before incubating with a panel of previously
586 titrated 14 barcoded oligo-conjugated antibodies (BioLegend TotalSeq-C), including FITC-anti-
587 CD45. Stained PBMC samples were then sorted by fluorescence activated cell sorting (FACS) on
588 a BD FACSMelody to enrich for live, hematopoietic cells. A standard viable CD45+ cell gating
589 scheme was employed; FSC-A v SSCA (to exclude sub-cellular debris), two FSC-A doublet
590 exclusion gates (FSC-W followed by FSC-H), dead cell exclusion gate (BV510 LIVE/DEAD negative)
591 followed by CD45+ inclusion gate.

592 Sorted cells were resuspended in PBS supplemented with 1% BSA. Cells were loaded onto the
593 10X Chromium system, where we aimed for recovery of ~5000 cells per sample, and subjected
594 to partitioning with barcoded 5' V1.1 chemistry gel-beads (10X Genomics) to generate the Gel-
595 Bead in Emulsions (GEMs). The RT reaction was conducted in the GEMs, barcoded cDNA
596 extracted by post-GEM RT-cleanup, and cDNA and antibody barcodes amplified with 14 cycles.
597 Amplified cDNA was subjected to SPRI bead cleanup at 0.6X. Amplified antibody barcodes were
598 recovered from the supernatant and were processed to generate TotalSeq-C libraries as
599 instructed by the manufacturers (10X Genomics and BioLegend, TotalSeq-C with 10x Feature
600 Barcoding Protocol). The remaining amplified cDNA was subjected to enzymatic fragmentation,
601 end-repair, A-tailing, adapter ligation and 10X specific sample indexing as per manufacturer's
602 protocol. Libraries were quantified using Bioanalyzer (Agilent) analysis. 10x Genomics scRNA-Seq
603 and TotalSeq-C libraries were pooled and sequenced on an Illumina NovaSeq Sp100 flow cell
604 using the recommended sequencing read lengths of 26 bp (Read 1), 8 bp (i7 Index Read), and 91

605 bp (Read 2), and depths of 50,000 and 5000 read pairs per cell for the 5' Gene Expression and
606 TotalSeq-C libraries respectively. Cell Ranger v3.1.0 (10x Genomics) was used to demultiplex raw
607 sequencing data and quantitate transcript levels against the 10x Genomics GRCh38 reference.

608

609 **Single-cell RNA seq processing and analysis**

610 Raw count data were filtered to remove cells where 1) a mitochondrial RNA fraction greater than
611 7.5% of total RNA counts per cell, and 2) less than 200 or greater than 2500 genes were detected.
612 The resultant count matrix was used to create a Seurat (v4.0.1) (Hao et al., 2021) object. Filtered
613 read counts were normalized, scaled, and corrected for mitochondrial and rRNA read
614 percentages with the SCTransform function. The ADT matrix was normalized per feature using
615 center log normalization. Cell types in each sample were annotated by mapping to the annotated
616 reference PBMC dataset provided in the Seurat v4 Azimuth workflow. Briefly, anchors between
617 the query and reference datasets were identified using a precomputed supervised PCA on the
618 reference dataset. Next, cell type labels from the reference dataset, as well as imputations of all
619 measured protein markers, were transferred to each cell of the query datasets through the
620 previously identified anchors. The query datasets were then merged and projected onto the
621 UMAP structure of the reference. The genes expressed in each specific cell cluster were identified
622 using the FindAllMarkers function from the Seurat4 package and filtered to include those with
623 average $\log_2$ fold changes greater than 1 and FDR-adjusted P-values less than 0.05.

624

625 **Acknowledgements**

626 We would like to thank Michael Gale and Nana Minkah for their helpful comments on the
627 manuscript. We would also like to acknowledge the contribution of all the IMRAS study
628 volunteers.

629

630 **Funding**

631 This work was supported by NIH grant U19AI128914 to KS and NIH grant P41GM109824 to JA.
632 The IMRAS trial at the Naval Medical Research Center and some RNAseq data collection was
633 funded by the Bill & Melinda Gates Foundation with grants OPP1034596 (under NMRC-12-3941
634 and NMRC-15-0579 CRADAs) and GHVAP NG-ID18-Stuart.

635

636 **Competing Interests**

637 The authors declare no competing interests exist

638 **References:**

639 Ali S, Mann-Nüttel R, Schulze A, Richter L, Alferink J, Scheu S. 2019. Sources of type I interferons
640 in infectious immunity: Plasmacytoid dendritic cells not always in the driver's seat. *Front*
641 *Immunol*. doi:10.3389/fimmu.2019.00778

642 Anders S, Pyl PT, Huber W. 2015. HTSeq-A Python framework to work with high-throughput
643 sequencing data. *Bioinformatics* **31**:166–169. doi:10.1093/bioinformatics/btu638

644 Bates D, Mächler M, Bolker BM, Walker SC. 2015. Fitting linear mixed-effects models using
645 lme4. *J Stat Softw* **67**:1–48. doi:10.18637/jss.v067.i01

646 Becker M, De Bastiani MA, Parisi MM, Guma FTCR, Markoski MM, Castro MAA, Kaplan MH,
647 Barbé-Tuana FM, Klamt F. 2015. Integrated Transcriptomics Establish Macrophage
648 Polarization Signatures and have Potential Applications for Clinical Health and Disease. *Sci*
649 *Rep* **5**:13351. doi:10.1038/srep13351

650 Chaussabel D, Quinn C, Shen J, Patel P, Glaser C, Baldwin N, Stichweh D, Blankenship D, Li L,
651 Munagala I, Bennett L, Allantaz F, Mejias A, Ardura M, Kaizer E, Monnet L, Allman W,
652 Randall H, Johnson D, Lanier A, Punaro M, Wittkowski KM, White P, Fay J, Klintmalm G,
653 Ramilo O, Palucka AK, Banchereau J, Pascual V. 2008a. A modular analysis framework for
654 blood genomics studies: application to systemic lupus erythematosus. *Immunity* **29**:150–
655 64. doi:10.1016/j.immuni.2008.05.012

656 Chaussabel D, Quinn C, Shen J, Patel P, Glaser C, Baldwin N, Stichweh D, Blankenship D, Li L,
657 Munagala I, Bennett L, Allantaz F, Mejias A, Ardura M, Kaizer E, Monnet L, Allman W,
658 Randall H, Johnson D, Lanier A, Punaro M, Wittkowski KM, White P, Fay J, Klintmalm G,
659 Ramilo O, Palucka AK, Banchereau J, Pascual V. 2008b. A Modular Analysis Framework for
660 Blood Genomics Studies: Application to Systemic Lupus Erythematosus. *Immunity* **29**:150–
661 164. doi:10.1016/j.immuni.2008.05.012

662 Cockburn IA, Amino R, Kelemen RK, Kuo SC, Tse S-W, Radtke A, Mac-Daniel L, Ganusov V V,
663 Zavala F, Menard R. 2013. In vivo imaging of CD8+ T cell-mediated elimination of malaria
664 liver stages. *Proc Natl Acad Sci* **110**:9090–9095. doi:10.1073/pnas.1303858110

665 Coelho CH, Doritchamou JYA, Zaidi I, Duffy PE. 2017. Advances in malaria vaccine development:
666 Report from the 2017 malaria vaccine symposiumNpj Vaccines. Nature Publishing Group.
667 doi:10.1038/s41541-017-0035-3

668 Collin M, Bigley V. 2018. Human dendritic cell subsets: an update. *Immunology*.
669 doi:10.1111/imm.12888

670 Costantini C, Cassatella MA. 2011. The defensive alliance between neutrophils and NK cells as a
671 novel arm of innate immunity. *J Leukoc Biol* **89**:221–233. doi:10.1189/jlb.0510250

672 de Paus RA, van Wengen A, Schmidt I, Visser M, Verdegaal EME, van Dissel JT, van de Vosse E.
673 2013. Inhibition of the type I immune responses of human monocytes by IFN-α and IFN-β.
674 *Cytokine* **61**:645–655. doi:10.1016/j.cyto.2012.12.005

675 Dobin A, Davis CA, Schlesinger F, Drenkow J, Zaleski C, Jha S, Batut P, Chaisson M, Gingeras TR.
676 2013. STAR: Ultrafast universal RNA-seq aligner. *Bioinformatics* **29**:15–21.
677 doi:10.1093/bioinformatics/bts635

678 Doolan DL, Hoffman SL. 2000. The Complexity of Protective Immunity Against Liver-Stage
679 Malaria. *J Immunol* **165**:1453–1462. doi:10.4049/jimmunol.165.3.1453

680 Epstein JE, Paolino KM, Richie TL, Sedegah M, Singer A, Ruben AJ, Chakravarty S, Stafford A,
681 Ruck RC, Eappen AG, Li T, Billingsley PF, Manoj A, Silva JC, Moser K, Nielsen R, Tosh D,
682 Cicatelli S, Ganeshan H, Case J, Padilla D, Davidson S, Garver L, Saverino E, Murshedkar T,
683 Gunasekera A, Twomey PS, Reyes S, Moon JE, James ER, Kc N, Li M, Abot E, Belmonte A,
684 Hauns K, Belmonte M, Huang J, Vasquez C, Remich S, Carrington M, Abebe Y, Tillman A,
685 Hickey B, Regules J, Villasante E, Sim BKL, Hoffman SL. 2017. Protection against
686 Plasmodium falciparum malaria by PfSPZ Vaccine. *JCI insight* **2**:e89154.
687 doi:10.1172/jci.insight.89154

688 Fernandez-Ruiz D, Ng WY, Holz LE, Ma JZ, Zaid A, Wong YC, Lau LS, Mollard V, Cozijnsen A,
689 Collins N, Li J, Davey GM, Kato Y, Devi S, Skandari R, Pauley M, Manton JH, Godfrey DI,
690 Braun A, Tay SS, Tan PS, Bowen DG, Koch-Nolte F, Rissiek B, Carbone FR, Crabb BS, Lahoud
691 M, Cockburn IA, Mueller SN, Bertolino P, McFadden GI, Caminschi I, Heath WR. 2016a.
692 Liver-Resident Memory CD8+ T Cells Form a Front-Line Defense against Malaria Liver-Stage
693 Infection. *Immunity* **45**:889–902. doi:10.1016/j.immuni.2016.08.011

694 Fernandez-Ruiz D, Ng WY, Holz LE, Ma JZ, Zaid A, Wong YC, Lau LS, Mollard V, Cozijnsen A,
695 Collins N, Li J, Davey GM, Kato Y, Devi S, Skandari R, Pauley M, Manton JH, Godfrey DI,
696 Braun A, Tay SS, Tan PS, Bowen DG, Koch-Nolte F, Rissiek B, Carbone FR, Crabb BS, Lahoud
697 M, Cockburn IA, Mueller SN, Bertolino P, McFadden GI, Caminschi I, Heath WR, Chun Y.
698 2016b. Supplemental Information Liver-Resident Memory CD8 + T Cells Form a Front-Line
699 Defense against Malaria Liver-Stage Infection. *Immunity* **45**:889–902.
700 doi:10.1016/j.immuni.2016.08.011

701 George VK, Pallikkuth S, Pahwa R, De Armas LR, Rinaldi S, Pan L, Pahwa S. 2018. Circulating
702 inflammatory monocytes contribute to impaired influenza vaccine responses in HIV-
703 infected participants. *AIDS* **32**:1219–1228. doi:10.1097/QAD.0000000000001821

704 Guarda G, Braun M, Staehli F, Tardivel A, Mattmann C, Förster I, Farlik M, Decker T, Du Pasquier
705 RA, Romero P, Tschopp J. 2011. Type I Interferon Inhibits Interleukin-1 Production and
706 Inflammasome Activation. *Immunity* **34**:213–223. doi:10.1016/j.immuni.2011.02.006

707 Hao Y, Hao S, Andersen-Nissen E, Mauck WM, Zheng S, Butler A, Lee MJ, Wilk AJ, Darby C, Zager
708 M, Hoffman P, Stoeckius M, Papalexi E, Mimitou EP, Jain J, Srivastava A, Stuart T, Fleming
709 LM, Yeung B, Rogers AJ, McElrath JM, Blish CA, Gottardo R, Smibert P, Satija R. 2021.
710 Integrated analysis of multimodal single-cell data. *Cell*. doi:10.1016/j.cell.2021.04.048

711 Haque A, Best SE, De Oca MM, James KR, Ammerdorffer A, Edwards CL, De Labastida Rivera F,
712 Amante FH, Bunn PT, Sheel M, Sebina I, Koyama M, Varelias A, Hertzog PJ, Kalinke U, Gun
713 SY, Rénia L, Ruedl C, MacDonald KPA, Hill GR, Engwerda CR. 2014. Type I IFN signaling in

714 CD8-DCs impairs Th1-dependent malaria immunity. *J Clin Invest* **124**:2483–2496.
715 doi:10.1172/JCI70698

716 Hart GT, Tran TM, Theorell J, Schlums H, Arora G, Rajagopalan S, Jules Sangala AD, Welsh KJ,
717 Traore B, Pierce SK, Crompton PD, Bryceson YT, Long EO. 2019. Adaptive NK cells in people
718 exposed to Plasmodium falciparum correlate with protection from malaria. *J Exp Med*
719 **216**:1280–1290. doi:10.1084/jem.20181681

720 Hayakawa Y, Screpanti V, Yagita H, Grandien A, Ljunggren H-G, Smyth MJ, Chambers BJ. 2004.
721 NK Cell TRAIL Eliminates Immature Dendritic Cells In Vivo and Limits Dendritic Cell
722 Vaccination Efficacy. *J Immunol* **172**:123–129. doi:10.4049/jimmunol.172.1.123

723 Hertoghs N, Schwedhelm K V., Stuart KD, McElrath MJ, De Rosa SC. 2020. OMIP-064: A 27-Color
724 Flow Cytometry Panel to Detect and Characterize Human NK Cells and Other Innate
725 Lymphoid Cell Subsets, MAIT Cells, and γδ T Cells. *Cytom Part A* **97**:1019–1023.
726 doi:10.1002/cyto.a.24031

727 Hickey B, Teneza-Mora N, Lumsden J, Reyes S, Sedegah M, Garver L, Hollingdale MR, Banania
728 JG, Ganeshan H, Dowler M, Reyes A, Tamminga C, Singer A, Simmons A, Belmonte M,
729 Belmonte A, Huang J, Inoue S, Velasco R, Abot S, Vasquez CS, Guzman I, Wong M, Twomey
730 P, Wojnarski M, Moon J, Alcorta Y, Maiolatesi S, Spring M, Davidson S, Chaudhury S,
731 Villasante E, Richie TL, Epstein JE. 2020. IMRAS—A clinical trial of mosquito-bite
732 immunization with live, radiation-attenuated P. falciparum sporozoites: Impact of
733 immunization parameters on protective efficacy and generation of a repository of
734 immunologic reagents. *PLoS One* **15**:e0233840. doi:10.1371/journal.pone.0233840

735 Hwang I, Zhang T, Scott JM, Kim AR, Lee T, Kakarla T, Kim A, Sunwoo JB, Kim S. 2012.
736 Identification of human NK cells that are deficient for signaling adaptor FcRγ and
737 specialized for antibody-dependent immune functions. *Int Immunol* **24**:793–802.
738 doi:10.1093/intimm/dxs080

739 Ishizuka AS, Lyke KE, DeZure A, Berry AA, Richie TL, Mendoza FH, Enama ME, Gordon IJ, Chang
740 L-JJ, Sarwar UN, Zephir KL, Holman LA, James ER, Billingsley PF, Gunasekera A, Chakravarty
741 S, Manoj A, Li M, Ruben AJ, Li T, Eappen AG, Stafford RE, K C N, Murshedkar T, DeCederfelt
742 H, Plummer SH, Hendel CS, Novik L, Costner PJMM, Saunders JG, Laurens MB, Plowe C V.,
743 Flynn B, Whalen WR, Todd JP, Noor J, Rao S, Sierra-Davidson K, Lynn GM, Epstein JE, Kemp
744 MA, Fahle GA, Mikolajczak SA, Fishbaugher M, Sack BK, Kappe SHII, Davidson SA, Garver
745 LS, Björkström NK, Nason MC, Graham BS, Roederer M, Sim BKL, Hoffman SL, Ledgerwood
746 JE, Seder RA, C NK, Murshedkar T, DeCederfelt H, Plummer SH, Hendel CS, Novik L, M
747 Costner PJ, Saunders JG, Laurens MB, Plowe C V., Flynn B, Whalen WR, Todd JP, Noor J,
748 Rao S, Sierra-Davidson K, Lynn GM, Epstein JE, Kemp MA, Fahle GA, Mikolajczak SA,
749 Fishbaugher M, Sack BK, I Kappe SH, Davidson SA, Garver LS, Björkström NK, Nason MC,
750 Graham BS, Roederer M, Kim Lee Sim B, Hoffman SL, Ledgerwood JE, Seder RA, Natasha
751 KC, Murshedkar T, DeCederfelt H, Plummer SH, Hendel CS, Novik L, Costner PJMM,
752 Saunders JG, Laurens MB, Plowe C V., Flynn B, Whalen WR, Todd JP, Noor J, Rao S, Sierra-
753 Davidson K, Lynn GM, Epstein JE, Kemp MA, Fahle GA, Mikolajczak SA, Fishbaugher M,

754 Sack BK, Kappe SHII, Davidson SA, Garver LS, Björkström NK, Nason MC, Graham BS,
755 Roederer M, Kim Lee Sim B, Hoffman SL, Ledgerwood JE, Seder RA. 2016. Protection
756 against malaria at 1 year and immune correlates following PfSPZ vaccination. *Nat Med*
757 **22**:614–623. doi:10.1038/nm.4110

758 Jensen MA, Yanowitch RN, Reder AT, White DM, Arnason BG. 2010. Immunoglobulin-like
759 transcript 3, an inhibitor of T cell activation, is reduced on blood monocytes during
760 multiple sclerosis relapses and is induced by interferon β2-1b. *Mult Scler* **16**:30–38.
761 doi:10.1177/1352458509352794

762 Kaushansky A, Metzger PG, Douglass AN, Mikolajczak SA, Lakshmanan V, Kain HS, Kappe SHI.
763 2013. Malaria parasite liver stages render host hepatocytes susceptible to mitochondria-
764 initiated apoptosis. *Cell Death Dis* **4**. doi:10.1038/cddis.2013.286

765 Kazmin D, Nakaya HI, Lee EK, Johnson MJ, Van Der Most R, Van Den Berg RA, Ballou WR,
766 Jongert E, Wille-Reece U, Ockenhouse C, Aderem A, Zak DE, Sadoff J, Hendriks J,
767 Wrammert J, Ahmed R, Pulendran B. 2017. Systems analysis of protective immune
768 responses to RTS,S malaria vaccination in humans. *Proc Natl Acad Sci U S A* **114**:2425–
769 2430. doi:10.1073/pnas.1621489114

770 Kim B, Kim TH. 2018. Fundamental role of dendritic cells in inducing Th2 responses. *Korean J*
771 *Intern Med*. doi:10.3904/kjim.2016.227

772 King T, Lamb T. 2015. Interferon-γ: The Jekyll and Hyde of Malaria. *PLoS Pathog*.
773 doi:10.1371/journal.ppat.1005118

774 Korotkevich G, Sukhov V, Budin N, Shpak B, Artyomov M, Sergushichev A. 2016. Fast gene set
775 enrichment analysis. *bioRxiv* 060012. doi:10.1101/060012

776 Kurup SP, Anthony SM, Hancox LS, Vijay R, Pewe LL, Moioffer SJ, Sompallae R, Janse CJ, Khan
777 SM, Harty JT. 2019. Monocyte-Derived CD11c + Cells Acquire Plasmodium from
778 Hepatocytes to Prime CD8 T Cell Immunity to Liver-Stage Malaria. *Cell Host Microbe*
779 **25**:565-577.e6. doi:10.1016/j.chom.2019.02.014

780 Kusmartsev S, Nefedova Y, Yoder D, Gabrilovich DI. 2004. Antigen-Specific Inhibition of CD8 + T
781 Cell Response by Immature Myeloid Cells in Cancer Is Mediated by Reactive Oxygen
782 Species . *J Immunol* **172**:989–999. doi:10.4049/jimmunol.172.2.989

783 Lee AJ, Chen B, Chew M V., Barra NG, Shenouda MM, Nham T, van Rooijen N, Jordana M,
784 Mossman KL, Schreiber RD, Mack M, Ashkar AA. 2017. Inflammatory monocytes require
785 type I interferon receptor signaling to activate NK cells via IL-18 during a mucosal viral
786 infection. *J Exp Med* **214**:1153–1167. doi:10.1084/jem.20160880

787 Li D, Chen Y, Liu H, Jia Y, Li F, Wang W, Wu J, Wan Z, Cao Y, Zeng R. 2020. Immune dysfunction
788 leads to mortality and organ injury in patients with COVID-19 in China: insights from ERS-
789 COVID-19 study. *Signal Transduct Target Ther* **5**:62. doi:10.1038/s41392-020-0163-5

790 Li S, Nakaya HI, Kazmin DA, Oh JZ, Pulendran B. 2013. Systems biological approaches to
791 measure and understand vaccine immunity in humans. *Semin Immunol*.

792 doi:10.1016/j.smim.2013.05.003

793 Li S, Rouphael N, Duraisingham S, Romero-Steiner S, Presnell S, Davis C, Schmidt DS, Johnson
794 SE, Milton A, Rajam G, Kasturi S, Carlone GM, Quinn C, Chaussabel D, Palucka a K,
795 Mulligan MJ, Ahmed R, Stephens DS, Nakaya HI, Pulendran B. 2014a. Molecular signatures
796 of antibody responses derived from a systems biology study of five human vaccines. *Nat*
797 *Immunol* **15**:195–204. doi:10.1038/ni.2789

798 Li S, Rouphael N, Duraisingham S, Romero-Steiner S, Presnell S, Davis C, Schmidt DS, Johnson
799 SE, Milton A, Rajam G, Kasturi S, Carlone GM, Quinn C, Chaussabel D, Palucka AK, Mulligan
800 MJ, Ahmed R, Stephens DS, Nakaya HI, Pulendran B. 2014b. Molecular signatures of
801 antibody responses derived from a systems biology study of five human vaccines. *Nat*
802 *Immunol* **15**:195–204. doi:10.1038/ni.2789

803 Liberzon A, Birger C, Thorvaldsdóttir H, Ghandi M, Mesirov JP, Tamayo P. 2015. The Molecular
804 Signatures Database (MSigDB) hallmark gene set collection. *Cell Syst* **1**:417–425.
805 doi:10.1016/j.cels.2015.12.004

806 Liehl P, Meireles P, Albuquerque IS, Pinkevych M, Baptista F, Mota MM, Davenport MP,
807 Prudêncio M. 2015. Innate immunity induced by Plasmodium liver infection inhibits
808 malaria reinfections. *Infect Immun* **83**:1172–1180. doi:10.1128/IAI.02796-14

809 Liehl P, Zuzarte-Luís V, Chan J, Zillinger T, Baptista F, Carapau D, Konert M, Hanson KK, Carret C,
810 Lassnig C, Müller M, Kalinke U, Saeed M, Chora AF, Golenbock DT, Strobl B, Prudêncio M,
811 Coelho LP, Kappe SH, Superti-Furga G, Pichlmair A, Vigário AM, Rice CM, Fitzgerald KA,
812 Barchet W, Mota MM. 2014. Host-cell sensors for Plasmodium activate innate immunity
813 against liver-stage infection. *Nat Med* **20**:47–53. doi:10.1038/nm.3424

814 Mair F, Prlic M. 2018. OMIP-044: 28-color immunophenotyping of the human dendritic cell
815 compartment. *Cytom Part A* **93**:402–405. doi:10.1002/cyto.a.23331

816 Mantovani A, Cassatella MA, Costantini C, Jaillon S. 2011. Neutrophils in the activation and
817 regulation of innate and adaptive immunity. *Nat Publ Gr*. doi:10.1038/nri3024

818 Marques-Da-Silva C, Poudel B, Baptista RP, Peissig K, Hancox LS, Shiau JC, Pewe LL, Shears MJ,
819 Kanneganti T-D, Sinnis P, Kyle DE, Gurung P, Harty JT, Kurup SP. 2021. Altered cleavage of
820 Caspase-1 in hepatocytes limits control of malaria in the liver. *Biorxiv*.
821 doi:10.1101/2021.01.28.427517

822 McCarthy DJ, Chen Y, Smyth GK. 2012. Differential expression analysis of multifactor RNA-Seq
823 experiments with respect to biological variation. *Nucleic Acids Res* **40**:4288–4297.
824 doi:10.1093/nar/gks042

825 McKinney EF, Cuthbertson I, Harris KM, Smilek DE, Connor C, Manferrari G, Carr EJ, Zamvil SS,
826 Smith KGC. 2021. A CD8+ NK cell transcriptomic signature associated with clinical outcome
827 in relapsing remitting multiple sclerosis. *Nat Commun* **12**. doi:10.1038/s41467-020-20594-
828 2

829 McNab F, Mayer-Barber K, Sher A, Wack A, O'Garra A. 2015. Type I interferons in infectious

830 disease. *Nat Rev Immunol* **15**:87–103. doi:10.1038/nri3787

831 McNamara HA, Cai Y, Wagle M V., Sontani Y, Roots CM, Miosge LA, O'Connor JH, Sutton HJ,
832 Ganusov V V., Heath WR, Bertolino P, Goodnow CG, Parish IA, Enders A, Cockburn IA.
833 2017. Up-regulation of LFA-1 allows liver-resident memory T cells to patrol and remain in
834 the hepatic sinusoids. *Sci Immunol* **2**. doi:10.1126/sciimmunol.aaj1996

835 Mehta P, McAuley DF, Brown M, Sanchez E, Tattersall RS, Manson JJ. 2020. COVID-19: consider
836 cytokine storm syndromes and immunosuppression. *Lancet*. doi:10.1016/S0140-
837 6736(20)30628-0

838 Miller JL, Sack BK, Baldwin M, Vaughan AM, Kappe SHII. 2014. Interferon-Mediated Innate
839 Immune Responses against Malaria Parasite Liver Stages. *Cell Rep* **7**:436–447.
840 doi:10.1016/j.celrep.2014.03.018

841 Minkah NK, Wilder BK, Sheikh AA, Martinson T, Wegmair L, Vaughan AM, Kappe SHII. 2019.
842 Innate immunity limits protective adaptive immune responses against pre-erythrocytic
843 malaria parasites. *Nat Commun* **10**:1–14. doi:10.1038/s41467-019-11819-0

844 Mitchell LA, Henderson AJ, Dow SW. 2012. Suppression of Vaccine Immunity by Inflammatory
845 Monocytes. *J Immunol* **189**:5612–5621. doi:10.4049/jimmunol.1202151

846 Mootha VK, Lindgren CM, Eriksson KF, Subramanian A, Sihag S, Lehar J, Puigserver P, Carlsson E,
847 Ridderstråle M, Laurila E, Houstis N, Daly MJ, Patterson N, Mesirov JP, Golub TR, Tamayo P,
848 Spiegelman B, Lander ES, Hirschhorn JN, Altshuler D, Groop LC. 2003. PGC-1α-responsive
849 genes involved in oxidative phosphorylation are coordinately downregulated in human
850 diabetes. *Nat Genet* **34**:267–273. doi:10.1038/ng1180

851 Nagai T, Devergne O, Mueller TF, Perkins DL, van Seventer JM, van Seventer GA. 2003. Timing of
852 IFN-β Exposure during Human Dendritic Cell Maturation and Naive Th Cell Stimulation Has
853 Contrasting Effects on Th1 Subset Generation: A Role for IFN-β-Mediated Regulation of IL-
854 12 Family Cytokines and IL-18 in Naive Th Cell Differentiation. *J Immunol* **171**:5233–5243.
855 doi:10.4049/jimmunol.171.10.5233

856 Obeng-Adjei N, Portugal S, Tran TM, Yazew TB, Skinner J, Li S, Jain A, Felgner PL, Doumbo OK,
857 Kayentao K, Ongoiba A, Traore B, Crompton PD. 2015. Circulating Th1-Cell-type Tfh Cells
858 that Exhibit Impaired B Cell Help Are Preferentially Activated during Acute Malaria in
859 Children. *Cell Rep* **13**:425–439. doi:10.1016/j.celrep.2015.09.004

860 Otsuka A, Nakajima S, Kubo M, Egawa G, Honda T, Kitoh A, Nomura T, Hanakawa S, Sagita
861 Moniaga C, Kim B, Matsuoka S, Watanabe T, Miyachi Y, Kabashima K. 2013. Basophils are
862 required for the induction of Th2 immunity to haptens and peptide antigens. *Nat Commun*
863 **4**:1–9. doi:10.1038/ncomms2740

864 Perez-Mazliah D, Langhorne J. 2014. CD4 T-cell subsets in malaria: Th1/Th2 revisited. *Front*
865 *Immunol*. doi:10.3389/fimmu.2014.00671

866 Phythian-Adams AT, Cook PC, Lundie RJ, Jones LH, Smith KA, Barr TA, Hochweller K, Anderton
867 SM, Hämmerling GJ, Maizels RM, MacDonald AS. 2010. CD11c depletion severely disrupts

868 Th2 induction and development in vivo. *J Exp Med* **207**:2089–2096.
869 doi:10.1084/jem.20100734

870 Piccioli D, Sbrana S, Melandri E, Valiante NM. 2002. Contact-dependent stimulation and
871 inhibition of dendritic cells by natural killer cells. *J Exp Med* **195**:335–341.
872 doi:10.1084/jem.20010934

873 Pichyangkul S, Spring MD, Yongvanitchit K, Kum-Arb U, Limsalakpetch A, Im-Erbsin R, Ubalee R,
874 Vanachayangkul P, Remarque EJ, Angov E, Smith PL, Saunders DL. 2017. Chemoprophylaxis
875 with sporozoite immunization in P. knowlesi rhesus monkeys confers protection and elicits
876 sporozoite-specific memory T cells in the liver. *PLoS One* **12**:e0171826.
877 doi:10.1371/journal.pone.0171826

878 Pillay J, Kamp VM, Van Hoffen E, Visser T, Tak T, Lammers JW, Ulfman LH, Leenen LP, Pickkers P,
879 Koenderman L. 2012. A subset of neutrophils in human systemic inflammation inhibits T
880 cell responses through Mac-1. *J Clin Invest* **122**:327–336. doi:10.1172/JCI57990

881 Portugal S, Moebius J, Skinner J, Doumbo S, Doumtabe D, Kone Y, Dia S, Kanakabandi K,
882 Sturdevant DE, Virtaneva K, Porcella SF, Li S, Doumbo OK, Kayentao K, Ongoiba A, Traore B,
883 Crompton PD. 2014. Exposure-Dependent Control of Malaria-Induced Inflammation in
884 Children. *PLoS Pathog* **10**. doi:10.1371/journal.ppat.1004079

885 Portugal S, Tipton CM, Sohn H, Kone Y, Wang J, Li S, Skinner J, Virtaneva K, Sturdevant DE,
886 Porcella SF, Doumbo OK, Doumbo S, Kayentao K, Ongoiba A, Traore B, Sanz I, Pierce SK,
887 Crompton PD. 2015. Malaria-associated atypical memory B cells exhibit markedly reduced
888 B cell receptor signaling and effector function. *Elife* **4**. doi:10.7554/eLife.07218

889 Rayamajhi M, Humann J, Penheiter K, Andreasen K, Lenz LL. 2010. Induction of IFN-αβ enables
890 Listeria monocytogenes to suppress macrophage activation by IFN-γ. *J Exp Med* **207**:327–
891 337. doi:10.1084/jem.20091746

892 Reece WHH, Pinder M, Gothard PK, Milligan P, Bojang K, Doherty T, Plebanski M, Akinwunmi P,
893 Everaere S, Watkins KR, Voss G, Tornieporth N, Alloueche A, Greenwood BM, Kester KE,
894 McAdam KPWJ, Cohen J, Hill AVS. 2004. A CD4+ T-cell immune response to a conserved
895 epitope in the circumsporozoite protein correlates with protection from natural
896 Plasmodium falciparum infection and disease. *Nat Med* **10**:406–410. doi:10.1038/nm1009

897 Rocha BC, Marques PE, Leoratti FM de S, Junqueira C, Pereira DB, Antonelli LR do V, Menezes
898 GB, Golenbock DT, Gazzinelli RT. 2015. Type I Interferon Transcriptional Signature in
899 Neutrophils and Low-Density Granulocytes Are Associated with Tissue Damage in Malaria.
900 *Cell Rep* **13**:2829–2841. doi:10.1016/j.celrep.2015.11.055

901 Rolfes V, Ribeiro LS, Hawwari I, Böttcher L, Rosero N, Maasewerd S, Santos MLS, Schmidt S V,
902 Rothe M, Stunden HJ, Carvalho LH, Fontes CJ, Arditi M, Latz E, Franklin BS. 2019. Platelets
903 Fuel the Inflammasome Activation of Innate Immune Cells. *SSRN Electron J*.
904 doi:10.2139/ssrn.3439682

905 RTSS Clinical Trials Partnership. 2015. Efficacy and safety of RTS,S/AS01 malaria vaccine with or

906 without a booster dose in infants and children in Africa: Final results of a phase 3,
907 individually randomised, controlled trial. *Lancet* **386**:31–45. doi:10.1016/S0140-
908 6736(15)60721-8

909 Schuster IS, Coudert JD, Andoniou CE, Degli-Esposti MA. 2016. "Natural Regulators": NK cells as
910 modulators of T cell immunity. *Front Immunol*. doi:10.3389/fimmu.2016.00235

911 Seder RA, Chang LJ, Enama ME, Zephir KL, Sarwar UN, Gordon IJ, Holman LSA, James ER,
912 Billingsley PF, Gunasekera A, Richman A, Chakravarty S, Manoj A, Velmurugan S, Li ML,
913 Ruben AJ, Li T, Eappen AG, Stafford RE, Plummer SH, Hendel CS, Novik L, Costner PJM,
914 Mendoza FH, Saunders JG, Nason MC, Richardson JH, Murphy J, Davidson SA, Richie TL,
915 Sedegah M, Sutamihardja A, Fahle GA, Lyke KE, Laurens MB, Roederer M, Tewari K, Epstein
916 JE, Sim BKL, Ledgerwood JE, Graham BS, Hoffman SL. 2013. Protection against malaria by
917 intravenous immunization with a nonreplicating sporozoite vaccine. *Science (80-)*
918 **341**:1359–1365. doi:10.1126/science.1241800

919 Serafini P, Carbley R, Noonan KA, Tan G, Bronte V, Borrello I. 2004. High-Dose Granulocyte-
920 Macrophage Colony-Stimulating Factor-Producing Vaccines Impair the Immune Response
921 through the Recruitment of Myeloid Suppressor Cells, CANCER RESEARCH.

922 Subramanian A, Tamayo P, Mootha VK, Mukherjee S, Ebert BL, Gillette MA, Paulovich A,
923 Pomeroy SL, Golub TR, Lander ES, Mesirov JP. 2005. Gene set enrichment analysis: A
924 knowledge-based approach for interpreting genome-wide expression profiles. *Proc Natl*
925 *Acad Sci U S A* **102**:15545–15550. doi:10.1073/pnas.0506580102

926 Sullivan BM, Juedes A, Szabo SJ, Von Herrath M, Glimcher LH. 2003. Antigen-driven effector
927 CD8 T cell function regulated by T-bet. *Proc Natl Acad Sci U S A* **100**:15818–15823.
928 doi:10.1073/pnas.2636938100

929 Tang H, Cao W, Kasturi SP, Ravindran R, Nakaya HI, Kundu K, Murthy N, Kepler TB, Malissen B,
930 Pulendran B. 2010. The T helper type 2 response to cysteine proteases requires dendritic
931 cell-basophil cooperation via ROS-mediated signaling. *Nat Immunol* **11**:608–617.
932 doi:10.1038/ni.1883

933 Thompson EG, Du Y, Malherbe ST, Shankar S, Braun J, Valvo J, Ronacher K, Tromp G, Tabb DL,
934 Alland D, Shenai S, Via LE, Warwick J, Aderem A, Scriba TJ, Winter J, Walzl G, Zak DE, Du
935 Plessis N, Loxton AG, Chegou NN, Lee M. 2017. Host blood RNA signatures predict the
936 outcome of tuberculosis treatment. *Tuberculosis* **107**:48–58.
937 doi:10.1016/j.tube.2017.08.004

938 Thorndike RL. 1953. Who belongs in the family? *Psychometrika* **18**:267–276.
939 doi:10.1007/BF02289263

940 Tjota MY, Sperling AI. 2014. Distinct dendritic cell subsets actively induce Th2 polarization. *Curr*
941 *Opin Immunol*. doi:10.1016/j.coi.2014.09.006

942 Tran TM, Bijker EM, Haks MC, Ottenhoff THMM, Visser L, Schats R, Venepally P, Lorenzi H,
943 Crompton PD, Sauerwein RW. 2019. Whole-blood transcriptomic signatures induced

944 during immunization by chloroquine prophylaxis and Plasmodium falciparum sporozoites.
945 *Sci Rep* **9**:8386. doi:10.1038/s41598-019-44924-7

946 Trieu A, Kayala MA, Burk C, Molina DM, Freilich DA, Richie TL, Baldi P, Felgner PL, Doolan DL.
947 2011. Sterile protective immunity to malaria is associated with a panel of novel P.
948 falciparum antigens. *Mol Cell Proteomics* **10**. doi:10.1074/mcp.M111.007948

949 Tse S-W, Radtke AJ, Espinosa DA, Cockburn IA, Zavala F. 2014. The chemokine receptor CXCR6 is
950 required for the maintenance of liver memory $CD8^+$ T cells specific for infectious
951 pathogens. *J Infect Dis* **210**:1508–16. doi:10.1093/infdis/jiu281

952 van Eeden C, Khan L, Osman MS, Tervaert JWC. 2020. Natural killer cell dysfunction and its role
953 in covid-19. *Int J Mol Sci* **21**:1–17. doi:10.3390/ijms21176351

954 Veeranki S, Duan X, Panchanathan R, Liu H, Choubey D. 2011. IFI16 protein mediates the anti-
955 inflammatory actions of the type-I interferons through suppression of activation of
956 caspase-1 by inflammasomes. *PLoS One* **6**. doi:10.1371/journal.pone.0027040

957 Vekemans J, Schellenberg D, Benns S, O'Brien K, Alonso P. 2021. Meeting report: WHO
958 consultation on malaria vaccine development, Geneva, 15–16 July 2019. *Vaccine*.
959 doi:10.1016/j.vaccine.2021.03.093

960 Vivier E, Tomasello E, Baratin M, Walzer T, Ugolini S. 2008. Functions of natural killer cells. *Nat*
961 *Immunol*. doi:10.1038/ni1582

962 Waschbisch A, Sanderson N, Krumbholz M, Vlad G, Theil D, Schwab S, Mäurer M, Derfuss T.
963 2014. Interferon beta and vitamin D synergize to induce immunoregulatory receptors on
964 peripheral blood monocytes of multiple sclerosis patients. *PLoS One* **9**.
965 doi:10.1371/journal.pone.0115488

966 Weiss DJ, Bertozzi-Villa A, Rumisha SF, Amratia P, Arambepola R, Battle KE, Cameron E,
967 Chestnutt E, Gibson HS, Harris J, Keddie S, Millar JJ, Rozier J, Symons TL, Vargas-Ruiz C, Hay
968 SI, Smith DL, Alonso PL, Noor AM, Bhatt S, Gething PW. 2021. Indirect effects of the
969 COVID-19 pandemic on malaria intervention coverage, morbidity, and mortality in Africa: a
970 geospatial modelling analysis. *Lancet Infect Dis* **21**:59–69. doi:10.1016/S1473-
971 3099(20)30700-3

972 Wherry EJ, Ha S-J, Kaech SM, Haining WN, Sarkar S, Kalia V, Subramaniam S, Blattman JN,
973 Barber DL, Ahmed R. 2007. Molecular signature of CD8+ T cell exhaustion during chronic
974 viral infection. *Immunity* **27**:670–84. doi:10.1016/j.immuni.2007.09.006

975 Zambello R, Barilà G, Manni S, Piazza F, Semenzato G. 2020. NK cells and CD38: Implication for
976 (Immuno)Therapy in Plasma Cell Dyscrasias. *Cells*. doi:10.3390/cells9030768

977 Zemans RL. 2018. Neutrophil-mediated T-cell suppression in influenza: Novel finding raising
978 additional questions. *Am J Respir Cell Mol Biol*. doi:10.1165/rcmb.2017-0425ED

979 Zhang X, Ing S, Fraser A, Chen M, Khan O, Zakem J, Davis W, Quinet R. 2013. Follicular helper T
980 cells: New insights into mechanisms of autoimmune diseases. *Ochsner J* **13**:131–139.

981 Zhao L, Wang H, Thomas R, Gao X, Bai H, Shekhar S, Wang S, Yang J, Zhao W, Yang X. 2020. NK
982 cells modulate T cell responses via interaction with dendritic cells in Chlamydophila
983 pneumoniae infection. *Cell Immunol* **353**:104132. doi:10.1016/j.cellimm.2020.104132

984 Zheng M, Gao Y, Wang G, Song G, Liu S, Sun D, Xu Y, Tian Z. 2020. Functional exhaustion of
985 antiviral lymphocytes in COVID-19 patients. *Cell Mol Immunol* **17**:533–535.
986 doi:10.1038/s41423-020-0402-2

987

988

989

990

991

992

993

994

995

996

997

998

999

1000

1001

1002

1003

1004

1005

1006

1007

1008

1009 **Figure Legends**

1010

1011 **Figure 1. Vaccine induced gene responses after the first immunization. A** Barplot and table
1012 showing numbers of vaccine-induced genes with increased (red) or decreased (green) expression
1013 over each time interval in all immunized subjects (ALL_UP, ALL_DN) (FDR < 0.2, p <0.05, 90% CI >
1014 0 or < 0). Darker colors indicate genes that differ significantly in expression between protected
1015 (P) and non-protected (NP) subjects (PROT_UP, PROT_DN). **B** Heatmap of modules significantly
1016 enriched for vaccine-induced genes. Each row represents a BTM, each column represents a time
1017 interval. Heatmap color shows hypergeometric effect size (ES) of a BTM enriched in genes with
1018 increased (red/positive ES) or decreased (blue/negative ES) expression. Non-significant BTMs are
1019 shown in white. Assignment of a BTM to a high-level annotation group is illustrated by a colored
1020 sidebar.

1021

1022 **Figure 2. Vaccine induced protection associated gene responses**. **A**,**C**. Heatmaps showing 1394
1023 protection-associated genes ordered by hierarchical clustering based on expression in P (**A)** and
1024 NP (**C**) subjects for each time interval. Black sidebars indicate genes associated with an IPA
1025 pathway or BTM. Colored sidebars indicate P and NP gene clusters. Expression values were z-
1026 score transformed in rows for visualization. **B,D**. Enriched BTMs and IPA pathways for clusters
1027 from P (**B**) and NP (**D**) subjects. X axis represents –log10(FDR) generated from hypergeometric
1028 tests. Color indicates assignment of a BTM module or IPA pathway to a high-level annotation
1029 group. **E**. Circos plot showing overlap between P and NP clusters, numbered to match **A** and **C,**
1030 and colored by cluster number (e.g: P_1, NP_1: green, P_2, NP_2:orange). **F**. Expression changes
1031 of type I interferon-associated genes in P and NP subjects over each interval.

1032

1033 **Figure 3. Gene set enrichment analysis after the first immunization in P and NP subjects. A**.
1034 Heatmap of GSEA normalized enrichments scores (NES) derived from BTM expression changes
1035 over each time interval. Red represents activated BTMs and blue represents down-regulated
1036 BTMs. Asterisks represent significant differences in expression between P and NP for a time
1037 interval (Mann Whitney U test. ****: p < 0.0001; ***: p < 0.001; **: p < 0.01; *: p < 0.05). BTM
1038 clusters derived from hierarchical clustering are indicated by numbers to the right of the
1039 heatmap. Black sidebar on the left represents BTMs also enriched in unsupervised clusters of
1040 protection associated genes in P and NP subjects (Fig 1 B). **B**. Relationships between BTMs within
1041 the four identified clusters. BTMs with shared genes are connected by lines and the node sizes
1042 correspond to the numbers of shared genes. Predominant cell-type module annotations for each
1043 cluster are shown.

1044

1045 **Figure 4. Cell type-associated responses after the first vaccination. A.** Heatmap showing cell
1046 type specific BTM GSEA NESs in P and NP subjects. **B.** Heatmap showing expression changes of

malaria responding neutrophil genes in P and NP subjects on the sampling day compared with the previous sampling day. Expression values were z-score transformed by row for visualization.

Figure 5. Temporal changes of specific cell types across time intervals in P and NP subjects. A-D. Changes in flow-cytometry measured PBMC sub-populations over time, relative to day 0. **A**. non-classical monocytes and ILT3+ monocytes **B.** DCs **C**. T cells **D.** NK cells. Points represent cell proportion values in each subject. Line represents average values across P and NP subjects. LMER p-values are shown for P vs NP differences. **E-G**. Flow cytometry gating schemes **E**. DC subsets and monocytes **F**. Th1 and Th2 cells **G**. NK cells.

Figure 6. Correlation of temporal changes between cell subsets and BTMs. A. Heatmap showing correlations between flow-cytometry derived cell subset counts from NK and DC panels (columns) and BTM expression (rows) matched by participant and time-point. Red represents positive correlation, blue represents negative correlation, and white represents non-significant correlations. Regions of positive and negative correlation are numbered 1-7. **B,C**. Changes over time (relative to day 0) of BTMs and cell subsets that are strongly positively correlated (**B**, blocks 1-4 in heatmap **A**) and negatively correlated (**C**, blocks 5-7 in heatmap A). Each line represents average expression changes (relative to day 0) of a cell subset or BTM in P and NP subjects.

Figure 7. Validation of transcriptional changes of specific cell types using CITEseq data. A Scatter plot illustrating cell types identified in CITEseq data, visualized using uniform manifold approximation and projection (UMAP). Each point represents a cell and is colored by cell type. **B** Heatmap showing GSEA NES of CITEseq-derived cell signatures in whole-blood RNAseq in response to the first immunization in P and NP subjects. **C.** Lineplot showing kinetics of CITEseq-identified cell signatures in P and NP subjects. Each line represents the median gene expression levels of a CITEseq gene signature per-subject, and the black dashed line represents the median gene expression levels across all in P or NP subjects. **D**. Heatmap showing Spearman's rank correlation between cell-type specific BTMs and CITEseq identified cell-specific signatures. The color row bar indicates cell-type annotation of BTMs.

1085 **Supplementary Material**
1086
1087 **Figure S1. Overview of the IMRAS trial. A.** Schematic indicating timing of vaccination and
1088 sampling. **B**. Kaplan-Meier curve showing the percentage of true immunized subjects who did not
1089 develop parasitemia after CHMI (green) and those who did (red). **C.** Number of infectious
1090 mosquito bites received by each subject at each immunization. Circles and triangles indicate non-
1091 protected and protected subjects, respectively. Red lines indicate the median number of
1092 infectious mosquito bites.
1093
1094 **Figure S2. Comparison of protection associated clusters P_1 and NP_1. A,B.** Gene overlap of IPA
1095 pathways and BTMs enriched in cluster P_1 (**A**) and NP_1 (**B**), Node sizes indicate numbers of
1096 genes in a BTM or IPA pathway, and line thickness indicates the numbers of shared genes
1097 between two nodes. **C.** Heatmap showing expression of 317 genes common in cluster 1 of P
1098 subjects and cluster 1 of NP subjects. Expression values were z-score transformed in rows for
1099 visualization.
1100
1101 **Figure S3. Expression changes in pattern-recognition receptor pathwaysxs. A,B** Heat maps of
1102 expression changes for MyD88-dependent toll-like receptor associated genes (**A**) and MyD88-
1103 independent toll-like receptor associated genes (B) in P and NP subjects. Genes shown were
1104 selected using Gene-ontology (GO) annotations GO:0002755 (MyD88 dependent TLR signalling
1105 pathway) and GO:0002756 (MyD88 independent TLR signalling pathway). Expression values were
1106 Z-score transformed in rows for visualization. **C**. Average gene expression of selected IPA
1107 pathways over time in P (green) and NP (red) subjects. Dots represent average gene expression
1108 values per-individuals and solid line represents the average gene expression of the IPA pathway
1109 across all participants.
1110
1111 **Figure S4. Expanded color legend showing IPA pathways and BTMs enriched in Fig. 2**
1112
1113 **Figure S5. Expression changes in reactive-oxygen species pathway genes. A**. Heatmap showing
1114 expression of Hallmark Reactive Oxygen Species (ROS) Pathway genes. Expression values were z-
1115 score transformed in rows for visualization. **B**. STRING-DB derived protein-protein interaction
1116 networks of ROS genes, colored by expression changes on day 1 compared to day 0 seperately
1117 for P and NP. **C**. Average expression profiles of genes of Hallmark Reactive Oxygen Species
1118 Pathway in P and NP subjects. Dots represent average expression in individuals and solid line
1119 represents the average expression of the pathway over all P or NP subjects.
1120
1121 **Figure S6. Expression changes in pathways associated with specific immune cell types: A-**
1122 **I.**Heatmaps showing expression of genes of cell-type specific pathways: Neutrophils (**A**),

1123 Monocytes (**B**), DCs (**C**), Platelets (**D**), T-cells (**E**), B cells (**F**), NK cells (**G**), classically activated
1124 macrophages (**H**) and alternatively activated macrophages (**I**). Expression values were z-score
1125 transformed in rows for visualization.
1126
1127 **Table S1.** Genes and pathways associated with hierarchical clustering of protection-associated
1128 genes
1129
1130 **Table S2.** List of antibodies used for high parameter flow cytometry. Three separate staining
1131 panels for the detection of DC subsets, monocytes, T cells and NK cells are shown.
1132
1133 **Table S3:** List of CITEseq antibodies
1134

A

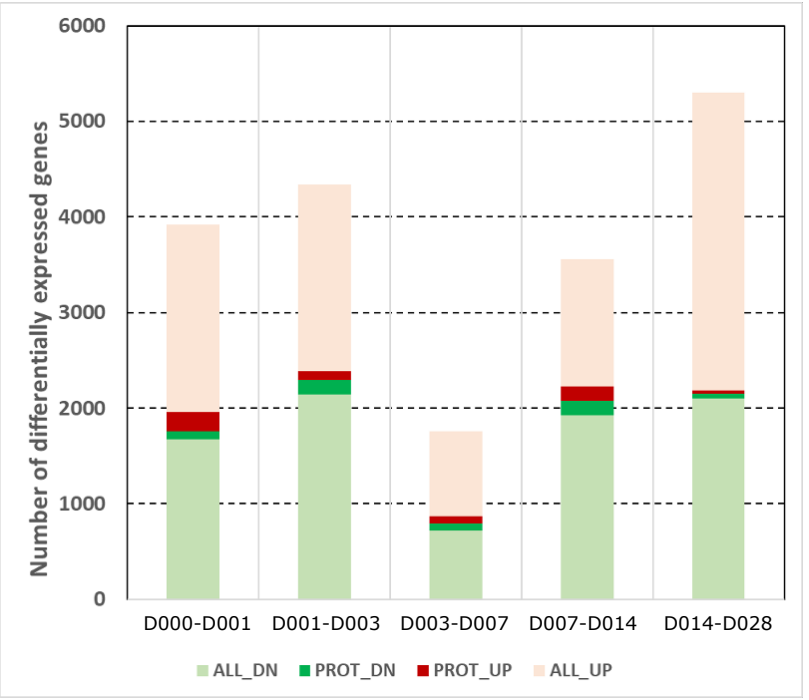

INTERVAL	ALL_UP	ALL_DN	PROT_UP	PROT_DN
D000-D001	1961	1669	208	84
D001-D003	1956	2138	91	152
D003-D007	885	714	76	81
D007-D014	1330	1925	148	151
D014-D028	3113	2103	36	45
#of unique genes	8170		806	

B

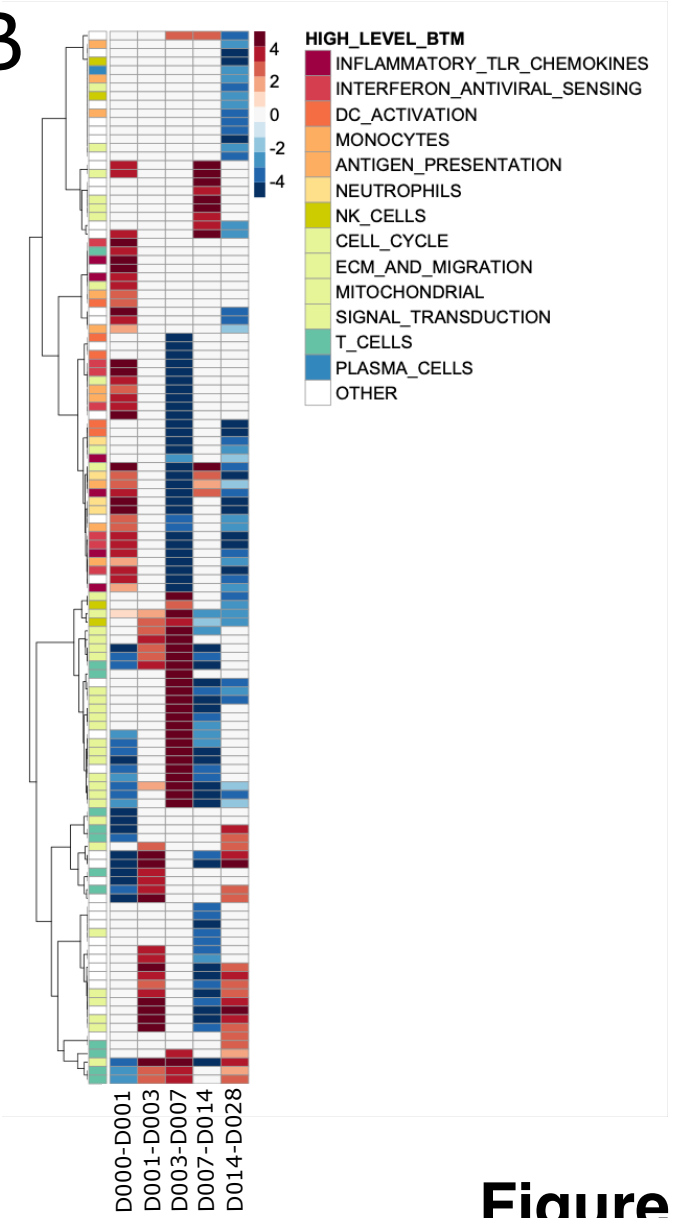

Figure 1

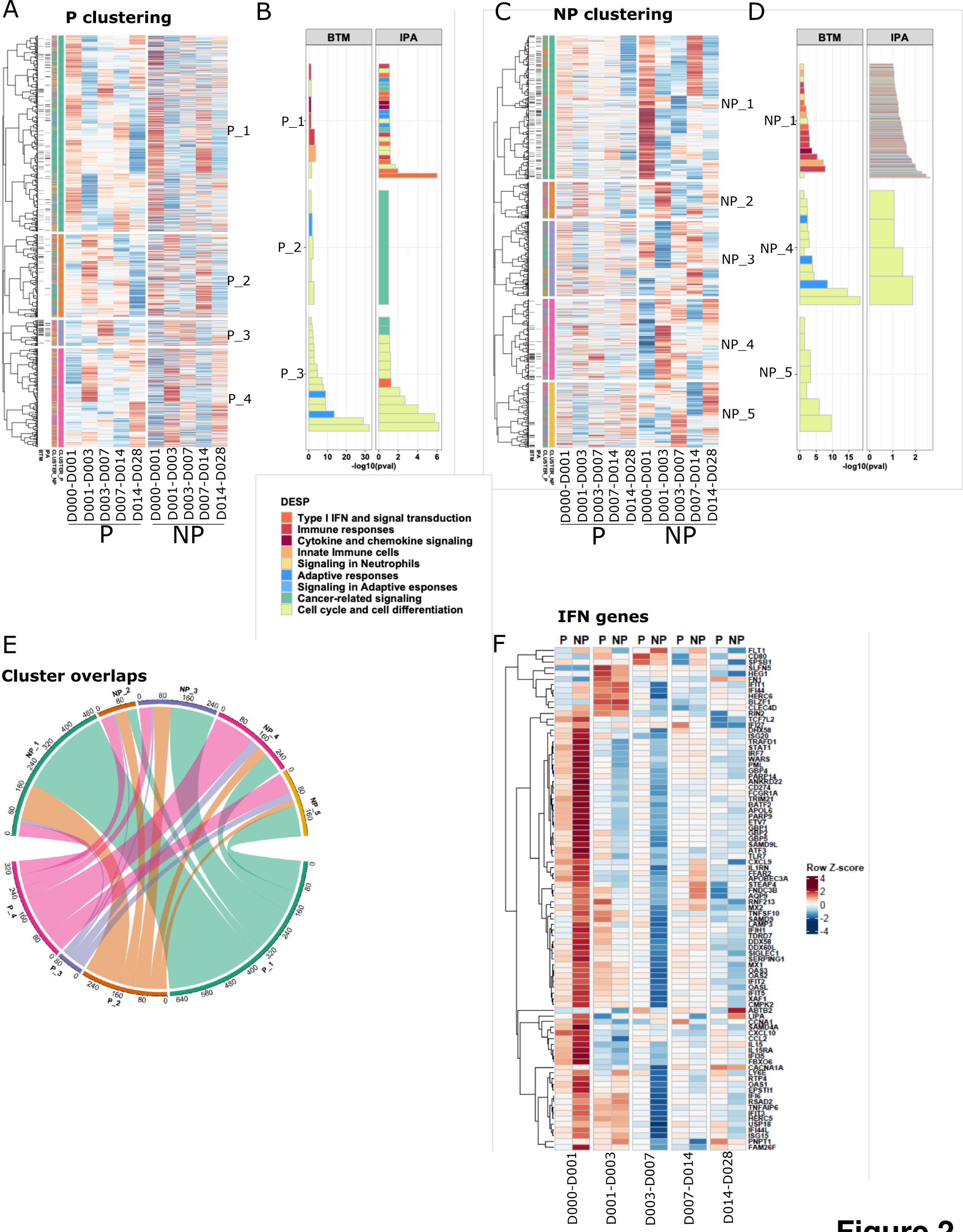
A
P clustering
P_1
P_2
P_3
P_4
D000-D001
D001-D003
D003-D007
D007-D014
D014-D028
P
NP
B
BTM
IPA
-log10(pval)
C
NP clustering
NP_1
NP_2
NP_3
NP_4
NP_5
D
DESP
Type I IFN and signal transduction
Immune responses
Cytokine and chemokine signaling
Innate Immune cells
Signaling in Neutrophils
Adaptive responses
Signaling in Adaptive esponses
Cancer-related signaling
Cell cycle and cell differentiation
E
Cluster overlaps
F
IFN genes
P NP
Row Z-score

Figure 2

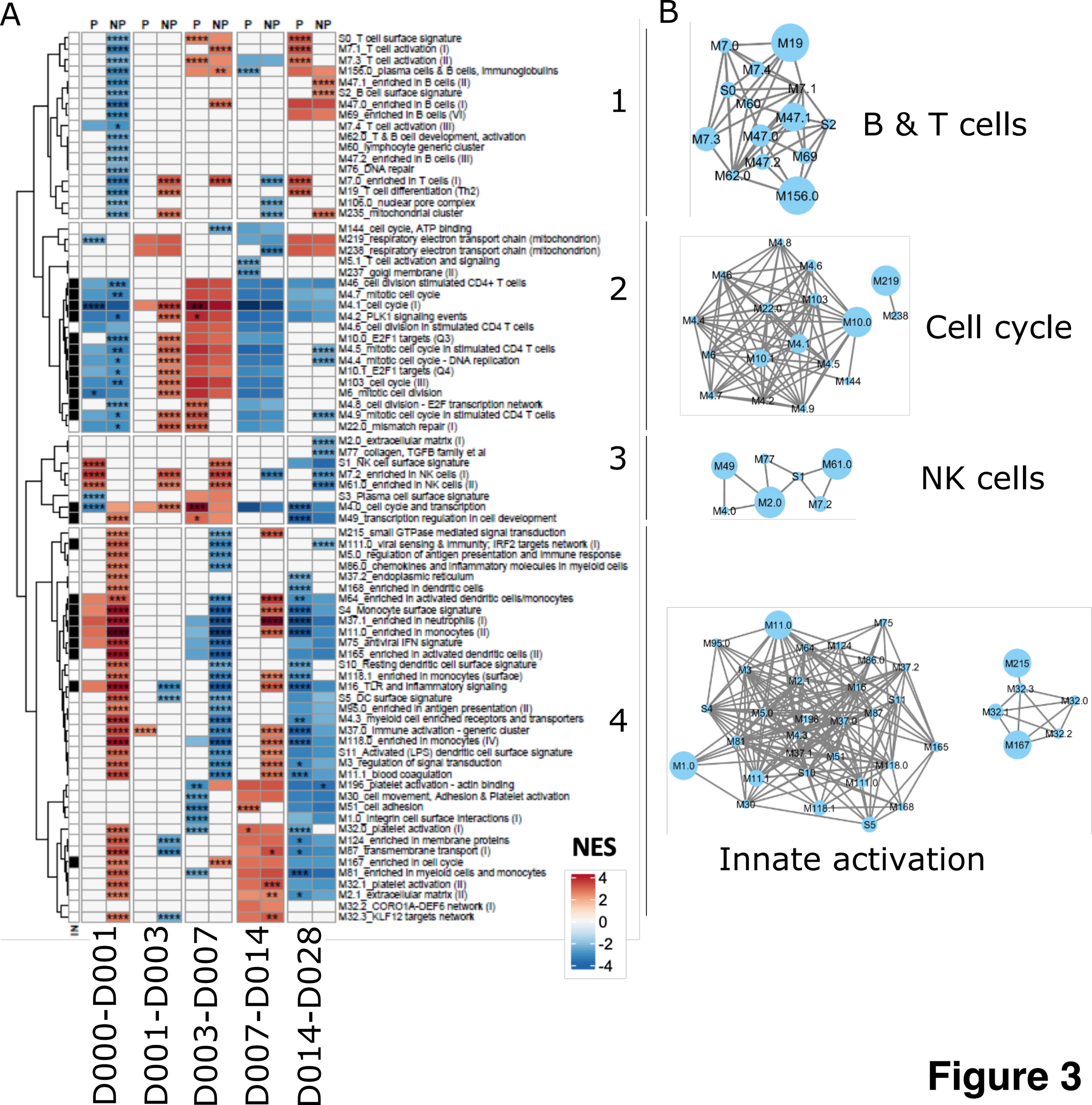
A
P NP P NP P NP P NP P NP
S0_T cell surface signature
M7.1_T cell activation (I)
M7.3_T cell activation (II)
M156.0_plasma cells & B cells, immunoglobulins
M47.1_enriched in B cells (II)
S2_B cell surface signature
M47.0_enriched in B cells (I)
M69_enriched in B cells (VI)
M7.4_T cell activation (III)
M62.0_T & B cell development, activation
M60_lymphocyte generic cluster
M47.2_enriched in B cells (III)
M76_DNA repair
M7.0_enriched in T cells (I)
M19_T cell differentiation (Th2)
M106.0_nuclear pore complex
M235_mitochondrial cluster
M144_cell cycle, ATP binding
M219_respiratory electron transport chain (mitochondrion)
M238_respiratory electron transport chain (mitochondrion)
M5.1_T cell activation and signaling
M237_golgi membrane (II)
M46_cell division stimulated CD4+ T cells
M4.7_mitotic cell cycle
M4.1_cell cycle (I)
M4.2_PLK1 signaling events
M4.6_cell division in stimulated CD4 T cells
M10.0_E2F1 targets (Q3)
M4.5_mitotic cell cycle in stimulated CD4 T cells
M4.4_mitotic cell cycle - DNA replication
M10.1_E2F1 targets (Q4)
M103_cell cycle (III)
M6_mitotic cell division
M4.8_cell division - E2F transcription network
M4.9_mitotic cell cycle in stimulated CD4 T cells
M22.0_mismatch repair (I)
M2.0_extracellular matrix (I)
M77_collagen, TGFB family et al
S1_NK cell surface signature
M7.2_enriched in NK cells (I)
M61.0_enriched in NK cells (II)
S3_Plasma cell surface signature
M4.0_cell cycle and transcription
M49_transcription regulation in cell development
M215_small GTPase mediated signal transduction
M111.0_viral sensing & immunity; IRF2 targets network (I)
M5.0_regulation of antigen presentation and immune response
M86.0_chemokines and inflammatory molecules in myeloid cells
M37.2_endoplasmic reticulum
M168_enriched in dendritic cells
M64_enriched in activated dendritic cells/monocytes
S4_Monocyte surface signature
M37.1_enriched in neutrophils (I)
M11.0_enriched in monocytes (II)
M75_antiviral IFN signature
M165_enriched in activated dendritic cells (II)
S10_Resting dendritic cell surface signature
M118.1_enriched in monocytes (surface)
M16_TLR and inflammatory signaling
S5_DC surface signature
M95.0_enriched in antigen presentation (II)
M4.3_myeloid cell enriched receptors and transporters
M37.0_immune activation - generic cluster
M118.0_enriched in monocytes (IV)
S11_Activated (LPS) dendritic cell surface signature
M3_regulation of signal transduction
M11.1_blood coagulation
M196_platelet activation - actin binding
M30_cell movement, Adhesion & Platelet activation
M51_cell adhesion
M1.0_integrin cell surface interactions (I)
M32.0_platelet activation (I)
M124_enriched in membrane proteins
M87_transmembrane transport (I)
M167_enriched in cell cycle
M81_enriched in myeloid cells and monocytes
M32.1_platelet activation (II)
M2.1_extracellular matrix (II)
M32.2_CORO1A-DEF6 network (I)
M32.3_KLF12 targets network
1
2
3
4
NES
4
2
0
-2
-4
D000-D001
D001-D003
D003-D007
D007-D014
D014-D028
B
M7.0
M19
M7.4
S0
M7.1
M60
M47.1
S2
M7.3
M47.0
M69
M47.2
M62.0
M156.0
B & T cells
M4.8
M4.6
M46
M219
M103
M22.0
M238
M4.4
M10.0
M4.1
M6
M10.1
M4.5
M144
M4.7
M4.2
M4.9
Cell cycle
M49
M77
M61.0
S1
M2.0
M7.2
M4.0
NK cells
M11.0
M75
M95.0
M64
M124
M86.0
M37.2
M3
M2.1
M16
S11
S4
M5.0
M196
M37.0
M87
M4.3
M81
M37.1
M51
M165
M1.0
M118.0
M11.1
S10
M111.0
M30
M118.1
M168
S5
M215
M32.3
M32.0
M32.1
M32.2
M167
Innate activation

Figure 3

A

Cell type BTMs

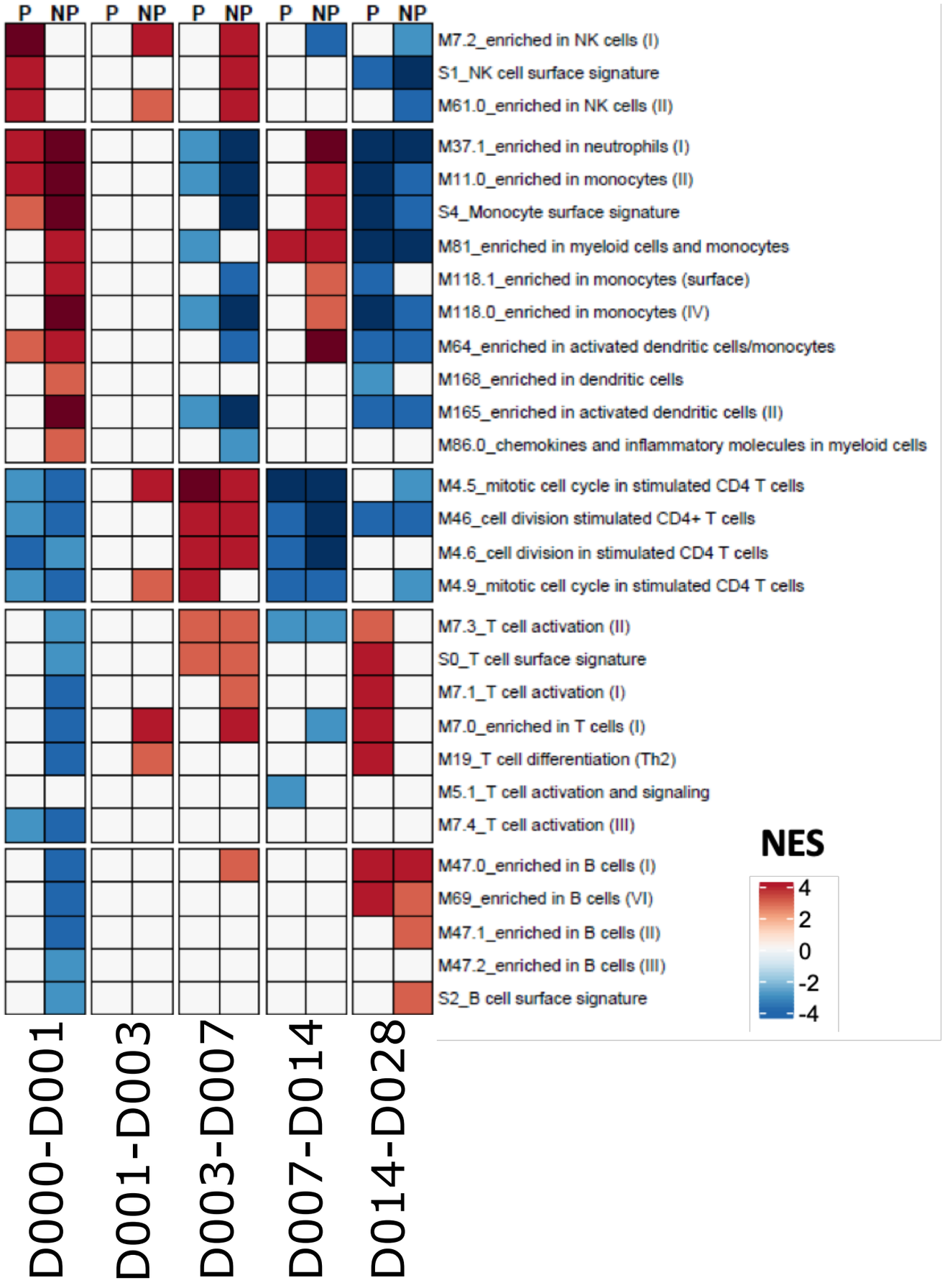

B

Neutrophil genes

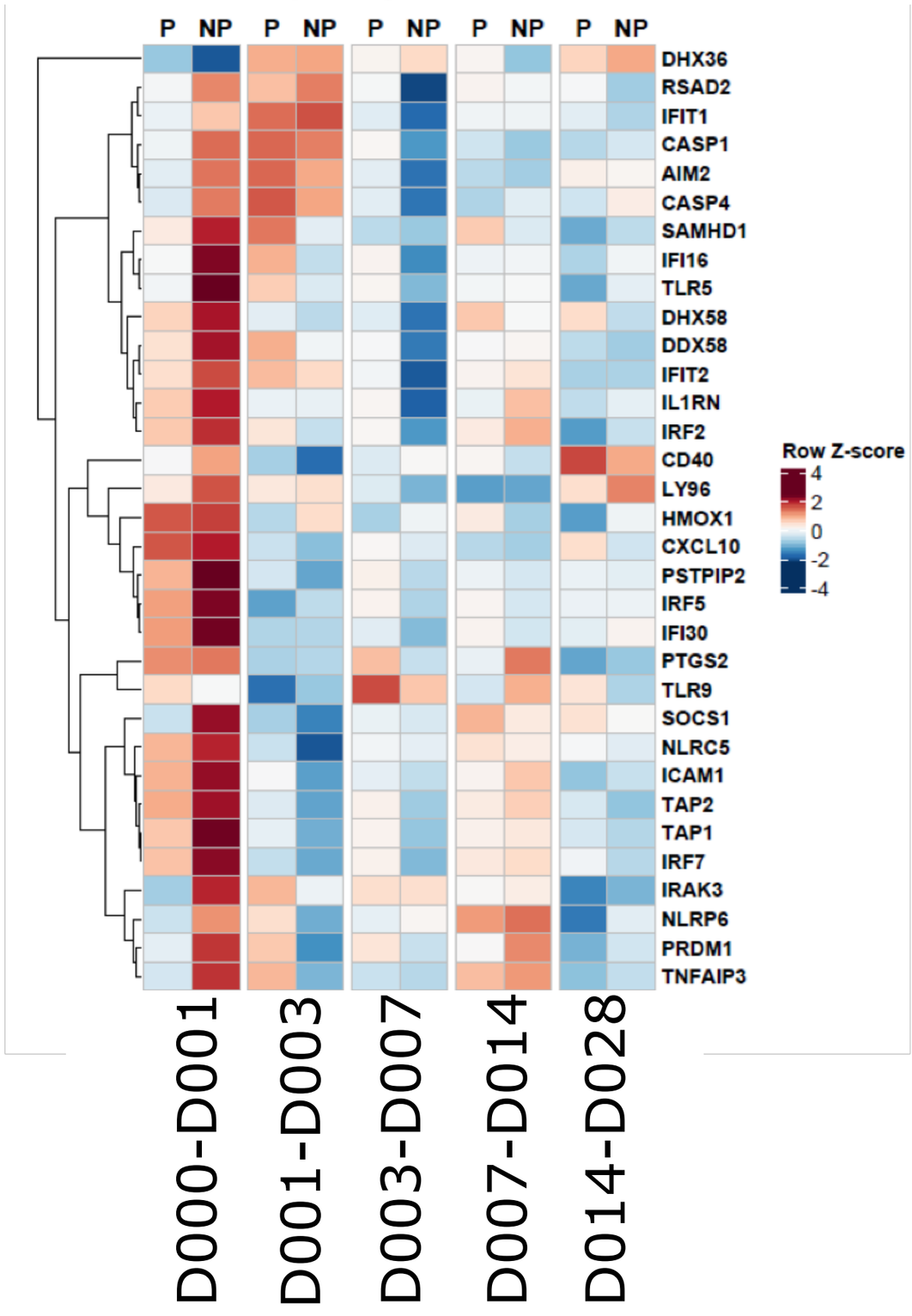

Figure 4

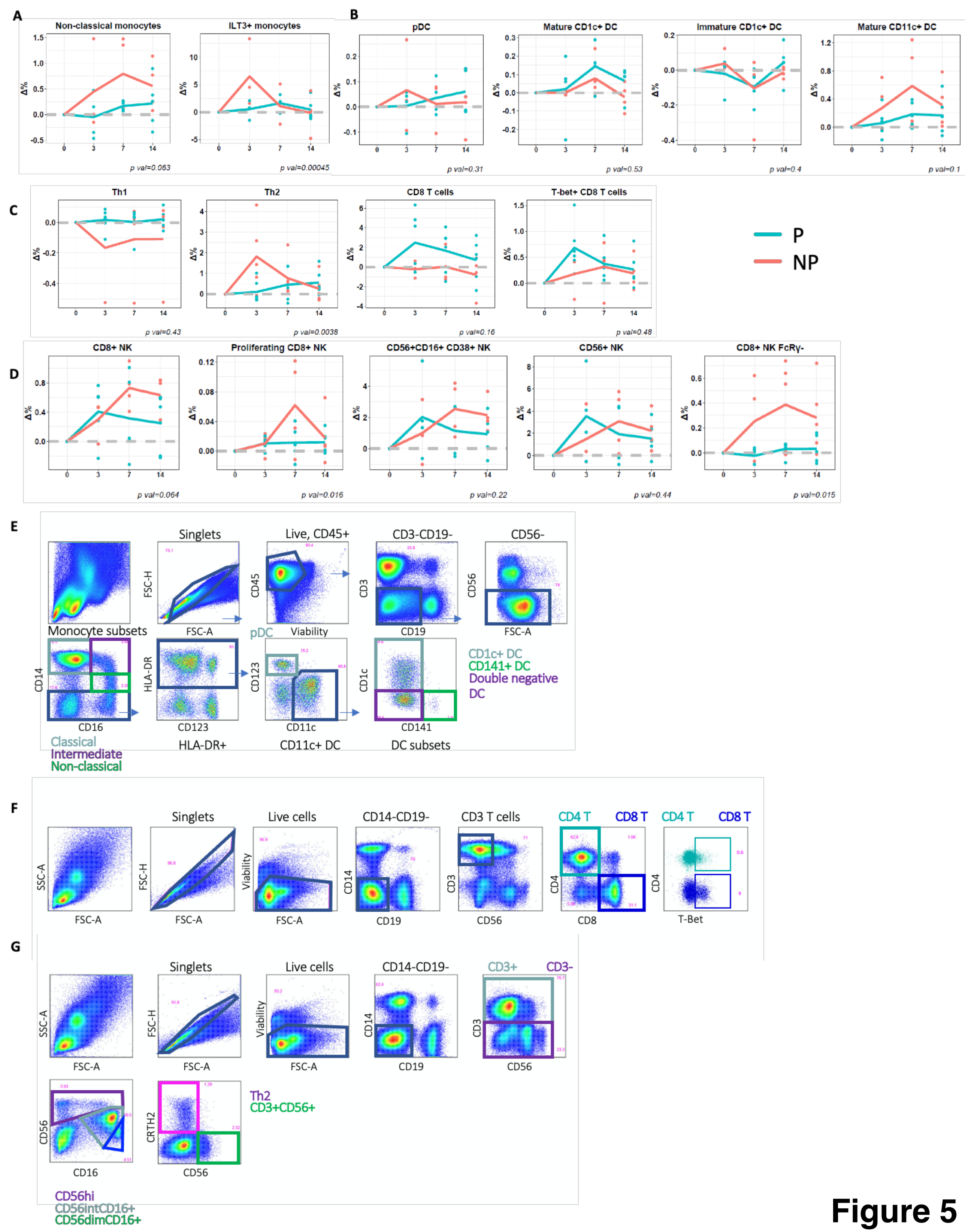
A
Non-classical monocytes
ILT3+ monocytes
p val=0.063
p val=0.00045
B
pDC
Mature CD1c+ DC
Immature CD1c+ DC
Mature CD11c+ DC
p val=0.31
p val=0.53
p val=0.4
p val=0.1
C
Th1
Th2
CD8 T cells
T-bet+ CD8 T cells
p val=0.43
p val=0.0038
p val=0.16
p val=0.48
P
NP
D
CD8+ NK
Proliferating CD8+ NK
CD56+CD16+ CD38+ NK
CD56+ NK
CD8+ NK FcRγ-
p val=0.064
p val=0.016
p val=0.22
p val=0.44
p val=0.015
E
Singlets
Live, CD45+
CD3-CD19-
CD56-
Monocyte subsets
pDC
CD1c+ DC
CD141+ DC
Double negative DC
Classical
Intermediate
Non-classical
HLA-DR+
CD11c+ DC
DC subsets
F
Singlets
Live cells
CD14-CD19-
CD3 T cells
CD4 T
CD8 T
CD4 T
CD8 T
G
Singlets
Live cells
CD14-CD19-
CD3+
CD3-
Th2
CD3+CD56+
CD56hi
CD56intCD16+
CD56dimCD16+

Figure 5

A

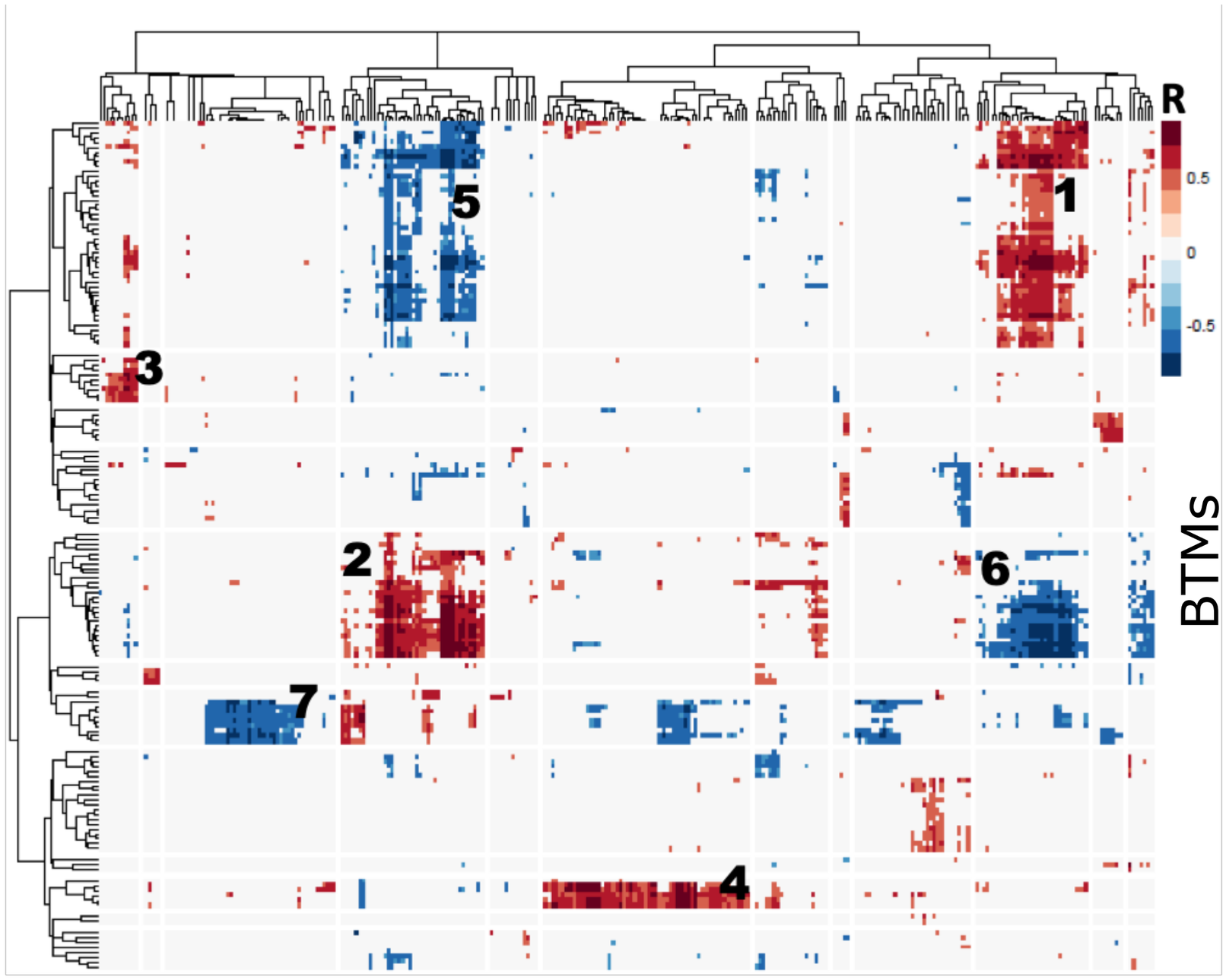

NK and DC subsets

B

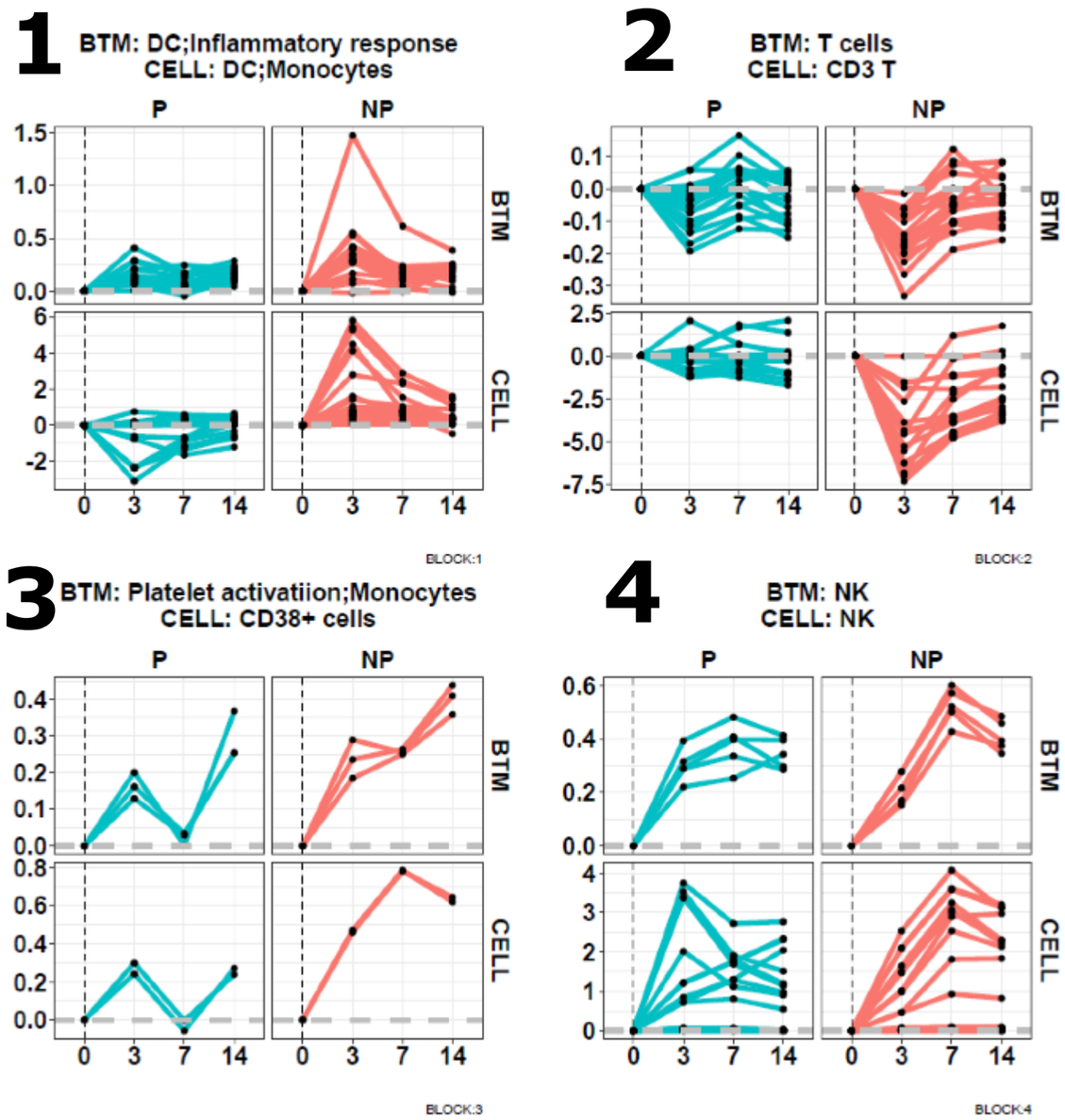

C

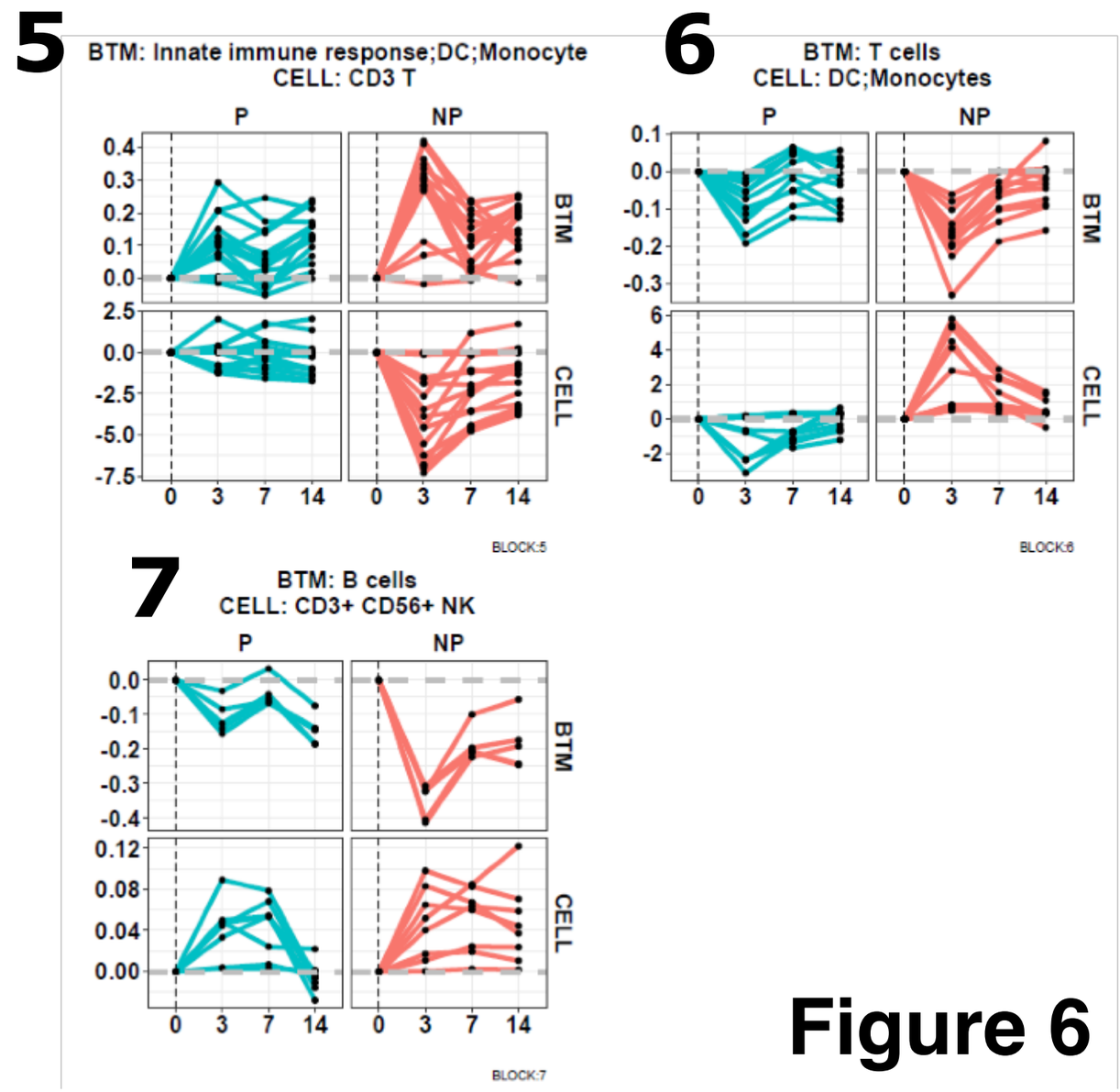

Figure 6

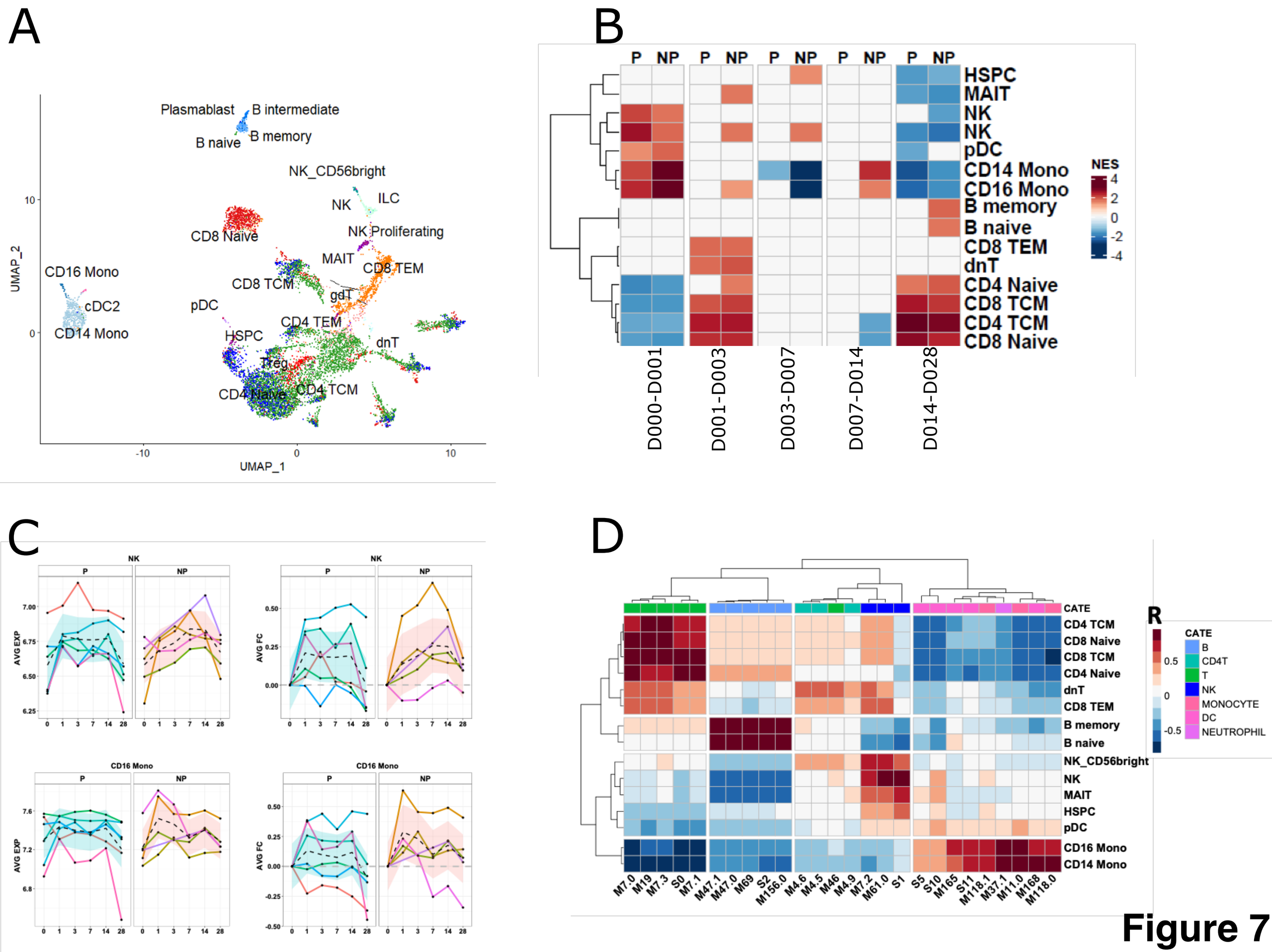
A
Plasmablast
B intermediate
B naive
B memory
NK_CD56bright
NK
ILC
NK Proliferating
CD8 Naive
MAIT
CD8 TEM
CD16 Mono
CD8 TCM
gdT
cDC2
pDC
CD4 TEM
CD14 Mono
HSPC
dnT
Treg
CD4 Naive
CD4 TCM
UMAP_2
UMAP_1
B
P NP P NP P NP P NP P NP
HSPC
MAIT
NK
NK
pDC
CD14 Mono
CD16 Mono
B memory
B naive
CD8 TEM
dnT
CD4 Naive
CD8 TCM
CD4 TCM
CD8 Naive
NES
D000-D001
D001-D003
D003-D007
D007-D014
D014-D028
C
NK
CD16 Mono
AVG EXP
AVG FC
P
NP
D
CATE
CD4 TCM
CD8 Naive
CD8 TCM
CD4 Naive
dnT
CD8 TEM
B memory
B naive
NK_CD56bright
NK
MAIT
HSPC
pDC
CD16 Mono
CD14 Mono
R
B
CD4T
T
NK
MONOCYTE
DC
NEUTROPHIL

Figure 7